https://doi.org/10.5194/essd-2020-209
Preprint. Discussion started: 16 October 2020

Status of the Tibetan Plateau observatory (Tibet-Obs) and a 10-year (2009-2019) surface soil moisture dataset

Pei Zhang[1,2], Donghai Zheng[2], Rogier van der Velde[1], Jun Wen[3], Yijian Zeng[1], Xin Wang[4], Zuoliang Wang[4], Jiali Chen[2,5], Zhongbo Su[1]

[1]Faculty of Geo-Information Science and Earth Observation (ITC), University of Twente, Enschede, 7514AE, the Netherlands
[2]National Tibetan Plateau Data Center, Key Laboratory of Tibetan Environmental Changes and Land Surface Processes, Institute of Tibetan Plateau Research, Chinese Academy of Sciences, Beijing, 100101, China
[3]College of Atmospheric Sciences, Chengdu University of Information Technology, Chengdu, 610225, China
[4]Northwest Institute of Eco-Environment and Resources, Chinese Academy of Sciences, Lanzhou, 730000, China
[5]College of Earth and Environmental Sciences, Lanzhou University, Lanzhou, 730000, China

Correspondence to: Donghai Zheng (zhengd@itpcas.ac.cn), Z. (Bob) Su (z.su@utwente.nl)

Abstract. The Tibetan Plateau observatory of plateau scale soil moisture and soil temperature (Tibet-Obs) was established ten years ago, which has been widely used to calibrate/validate satellite- and model-based soil moisture (SM) products for their applications to the Tibetan Plateau (TP). This paper reports on the status of the Tibet-Obs and presents a 10-year (2009-2019) surface SM dataset produced based on *in situ* measurements taken at a depth of 5 cm collected from the Tibet-Obs that consists of three regional-scale SM monitoring networks, i.e. the Maqu, Naqu, and Ngari (including Ali and Shiquanhe) networks. This surface SM dataset includes the original 15-min *in situ* measurements collected by multiple SM monitoring sites of the three networks, and the spatially upscaled SM records produced for the Maqu and Shiquanhe networks. Comparisons between four spatial upscaling methods, i.e. arithmetic averaging, Voronoi diagram, time stability and apparent thermal inertia, show that the arithmetic average of the monitoring sites with long-term (i.e. ≥ six years) continuous measurements are found to be most suitable to produce the upscaled SM records. Trend analysis of the 10-year upsclaed SM records using the Mann-Kendall method shows that the Maqu network area in the eastern part of the TP is drying while the Shiquanhe network area in the west is getting wet that generally follow the change of precipitation. To further demonstrate the uniqueness of the upscaled SM records in validating existing SM products for long term period (~10 years), comparisons are conducted to evaluate the reliability of three reanalysis datasets for the Maqu and Shiquanhe network areas. It is found that current model-based SM products still show deficiencies in representing the trend and variation of measured SM dynamics in the Tibetan grassland (i.e. Maqu) and desert ecosystems (i.e. Shiquanhe) that dominate the landscape of the TP. The dataset would be also valuable for calibrating/validating long-term satellite-based SM products, evaluation of SM upscaling methods, development of data fusion methods, and quantifying the coupling strength between precipitation and SM at 10-year scale. The dataset is available in the 4TU.ResearchData repository at https://doi.org/10.4121/uuid:21220b23-ff36-4ca9-a08f-ccd53782e834 (Zhang et al., 2020).

https://doi.org/10.5194/essd-2020-209
Preprint. Discussion started: 16 October 2020

1 Introduction

The Tibetan Plateau observatory (Tibet-Obs) of plateau scale soil moisture and soil temperature (SMST) was setup in 2006 and became fully operational in 2010 to calibrate/validate satellite- and model-based soil moisture (SM) products at regional scale (Su et al., 2011). The Tibet-Obs mainly consists of three regional-scale SMST monitoring networks, i.e. Maqu, Naqu, and Ngari, which cover different climate and land surface conditions across the Tibetan Plateau (TP) and include multiple *in situ* SMST monitoring sites in each network. The SM data collected from the Tibet-Obs have been widely used in past decade to calibrate/validate satellite- and model-based SM products (e.g. Su et al., 2013; Zheng et al., 2015a; Colliander et al., 2017), and to evaluate and develop SM upscaling methods (e.g. Qin et al., 2013; 2015), SM retrieval algorithms for microwave remote sensing (e.g. van der Velde et al., 2012; Zheng et al., 2018a; 2018b; 2019) and fusion methods to merge *in situ* SM and satellite- or model-based products (e.g. Yang et al., 2020; Zeng et al., 2016). Key information and outcomes of the main scientific applications using the Tibet-Obs SM data are summarized in Table 1. As shown in Table 1, the state-of-the-art satellite- and model-based products are useful but still show deficiencies of different degrees in different hydrometeorological conditions on the TP, and further evaluation and improvement of the latest versions of these products remain imperative. In general, previous studies mainly focused on the evaluation of SM products using the Tibet-Obs data for short term period (i.e. less than five years), while up to now the Tibet-Obs have collected *in situ* measurements more than 10 years. Development of an approximate 10-year *in situ* SM dataset collected from the Tibet-Obs would further enhance the calibration/validation of long-term satellite- and model-based products, and should be valuable for better understanding the hydrometeorological response to climate changes. However, the SM is highly variable in both space and time, and data gaps in the availability of measurements taken from individual monitoring site hinder scientific studies of longer periods, e.g. more than five years. Therefore, it is still challenging to obtain accurate long-term regional-scale SM due to the sparse nature of monitoring networks and highly variable soil conditions.

Spatial upscaling is usually necessary to obtain the regional-scale SM of an *in situ* network from multiple monitoring sites to match the scale of satellite- or model-based products. A frequently used approach for upscaling point-scale SM measurements to a spatial domain is the arithmetic average, mostly because of its simplicity (Su et al. 2011; 2013). Studies have also reported on application of a weighted averaging whereby the weights are chosen to account for spatial heterogeneity covered by the multiple monitoring sites within an *in situ* network. For instance, Colliander et al. (2017) employed Voronoi diagrams for the worldwide validation of the Soil Moisture Active/Passive (SMAP) SM products to determine the weights of individual monitoring sites within core regional-scale networks based on the geographic location; Dente et al. (2012a) determined the weights based on the topography and soil texture for the Maqu SM monitoring network of the Tibet-Obs; Qin et al. (2013) derived the weights by minimizing a cost function between *in situ* SM of individual monitoring site and a representative SM of the network that is estimated by the apparent-thermal-inertia-based (ATI) method. In addition, several particular or alternative methods, e.g. time stability (Zhao et al., 2013) and ridge regression (Kang et al., 2017) were also adopted in some investigations. The reliability

https://doi.org/10.5194/essd-2020-209
Preprint. Discussion started: 16 October 2020

of different spatial upscaling methods has been scarcely assessed for producing long-term consistent upscaled SM dataset for the *in situ* networks within which the number of individual monitoring sites changes over time due to damage of existing SM sensors, such as the Tibet-Obs.

This paper reports on the status of the Tibet-Obs and presents a long-term *in situ* SM and spatially upscaled SM dataset for the period between 2009 and 2019. The 10-year SM dataset includes the original 15-min *in situ* measurements taken at a depth of 5 cm collected from the three regional-scale networks (i.e. Maqu, Naqu, and Ngari) of the Tibet-Obs, and the consistent regional-scale SM produced by an appropriately selected spatial upscaling method. To achieve this aim, the performance of four spatial upscaling methods is investigated, including the arithmetic averaging (AA), Voronoi diagram (VD), time stability (TS) and apparent thermal inertia (ATI) methods. In addition, the Mann-Kendall (M-K) analysis is adopted to analyse the trend of both regional-scale SM and precipitation time series. Moreover, the regional-scale SM are used to validate the performance of three model-based SM products, e.g. ERA5-land (Albergel et al., 2018), MERRA2 (Modern-Era Retrospective Analysis for Research and Applications, version 2) (Gelaro et al., 2017), and GLDAS Noah (Global Land Data Assimilation System with Noah Land Surface Model) (Rodell et al., 2004), to demonstrate the uniqueness of this dataset for validating existing reanalysis datasets for long term period (~10 years).

This paper is organized as follows. Section 2 describes the status of the Tibet-Obs and *in situ* SM measurements, as well as the precipitation data and the three model-based SM products. Section 3 introduces the four SM spatial upscaling methods and the Mann-Kendall trend analysis method. Section 4 presents the inter-comparison of the four SM spatial upscaling methods, the production and analysis of regional-scale SM dataset for a 10-year period, and its application to validate the three model-based SM products. Section 5 provides the discussion and suggestion on maintaining the Tibet-Obs. Section 6 documents the information of data availability. Finally, conclusions are drawn in Section 7.

2 Data

2.1 Status of the Tibet-Obs

The Tibet-Obs consist of the Maqu, Naqu, and Ngari (including Shiquanhe and Ali) regional-scale SMST monitoring networks (Fig. 1) that cover different climate, vegetation, and soil conditions on the TP (Table 2). Brief descriptions of each network and corresponding surface SM measurements taken at a depth of 5 cm are given below, and the readers are referred to existing literature (Su et al., 2011; Dente et al. 2012a) for additional information.

2.1.1 Maqu network

The Maqu network is located in the north-eastern edge of the TP (33°30'-34°15'N, 101°38'-102°45'E) at the first major bend of the Yellow River. The landscape is dominated by the grassland at elevations varying from 3400 to 3800 m. The climate type is characterized as cold-humid with cold dry winters and rainy summers.

The mean annual air temperature is about 1.2 °C, with -10 °C for the coldest month (January) and 11.7 °C for the warmest month (July) (Zheng et al., 2015a). The soil texture is mainly silt loam at the surface layer with different amounts of organic matter content.

The Maqu network covers an area of approximately 40 by 80 km^2 and consists originally of 20 SMST monitoring sites installed in 2008 (Dente et al. 2012a). During the period between 2014 and 2016, eight new sites were installed due to the damage of several old sites by local people or animals. The SMST data are measured at different depths (5, 10, 20, 40, and 80 cm) for each site with 15/30 min intervals using the Decagon 5TM probes. Table 3 provides the specific periods of data missing during each year and the total data lengths of surface SM for each site. Among these sites, the CST05, NST01, and NST03 have collected more than nine years of SMST measurements, while the data records for the NST21, NST22, and NST31 are less than one year. In May 2019, there are still 12 sites that provided SMST data.

2.1.2 Ngari network

The Ngari network is located in the western part of the TP at the headwater of the Indus River. It consists of two SMST networks established around the cities of Ali and Shiquanhe, respectively (Fig. 1). The landscape is dominated by a desert ecosystem at elevations varying from 4200 to 4700 m. The climate type is characterized as cold-arid with a mean annual air temperature of 7.0 °C. The annual precipitation is less than 100 mm that falls mainly in the monsoon season (July-August) (van der Velde et al., 2014). The soil texture is characterized as fine sand with gravel at upper soil layers. Similar to the Maqu network, the SMST data of the Ali and Shiquanhe networks are also measured at nominal depths of 5, 10, 20, 40, and 80 cm with the Decagon 5TM probes at 15 min intervals.

The Shiquanhe network consists originally of 16 SMST monitoring sites installed in 2010 (Su et al. 2011), and five new sites were installed in 2016. Table 4 provides the specific periods of data missing during each year and the total data lengths of surface SM for each site. Among these sites, the SQ02, SQ03, SQ06, and SQ14 have collected more than eight years of SMST measurements, while the data records for the SQ13, SQ15, and SQ18 are less than two years. On August 2019, there are still 12 sites that provided SMST data.

The Ali network comprise four SMST monitoring sites (Table 4), which will thus not be used for the further analysis in this study due to limited number of sites and data records.

2.1.3 Naqu network

The Naqu network is located in the Naqu river basin with an average elevation of 4500 m. The landscape is dominated by the grassland, and the climate type is characterized as cold-semiarid with cold dry winters and rainy summers. Over three-quarters of total annual precipitation (400 mm) falls between June and August (Su et al., 2011). The soil texture is loamy sand with gravel and organic matter content in the root zone.

The network consists originally of five SMST monitoring sites installed in 2006 (Su et al. 2011), and six new sites were installed between 2010 and 2016. The SMST data are also measured at different depths (5/2.5, 10/7.5, 15, 30, and 60 cm) for each site with 15 min intervals using the Decagon 5TM probes. Table 5

https://doi.org/10.5194/essd-2020-209
Preprint. Discussion started: 16 October 2020

provides the specific periods of data missing during each year and the total data lengths of surface SM for each site. Among these sites, only the Naqu and MS have collected more than six years of SMST measurements, while the data records for the others are less than four years. Similar to the Ali network, the Naqu network will also not be used for the further analysis in this study due to limited number of sites and data records.

2.2 Precipitation data

The daily precipitation data from two weather stations (Fig. 1), i.e. Maqu (34°00'N, 102°05'E) and Shiquanhe (32°30'N, 80°50'E), operated by the China Meteorological Administration (CMA) are also collected. The CMA observational datasets are available from the China Meteorological Data Service Center (CMDC, http://data.cma.cn/en) that provides the near-surface meteorological data of about 700 weather stations in China.

2.3 Model-based soil moisture products

2.3.1 ERA5-land soil moisture product

The ERA5 is the latest generation of atmospheric reanalysis dataset produced by ECMWF (Albergel et al., 2018). The ERA5-land is based on running the land component of the model that is driven by the atmospheric analysis of ERA5 (Muñoz-Sabater et al., 2018). It uses the Tiled ECMWF Scheme for Surface Exchanges over Land incorporating land surface hydrology (H-TESSEL, CY45R1). The product provides SM data currently available from 1981 to 2-3 months before the present at hourly time interval with a finer spatial resolution (~9 km) that is freely accessed at https://www.ecmwf.int/en/era5-land. In this study, the data of volumetric total soil water content for the top soil layer (0-7 cm) is used for the analysis.

2.3.2 MERRA2 soil moisture product

The MERRA2 is a widely used atmospheric reanalysis dataset produced by NASA using advanced GEOS-5 model (Goddard Earth Observing System Model version5) and GSI (Gridpoint Statistical Interpolation) assimilation system (Gelaro et al., 2017). It is driven by observation-based precipitation data instead of model-generated precipitation in comparison to the MERRA products (1979-2016). The product provides SM data currently available from 1980 to the present with a spatial resolution of 0.5° lat by 0.625° lon at daily scale that is freely accessed at https://gmao.gsfc.nasa.gov/reanalysis/MERRA-2. In this study, the data of volumetric liquid soil water content for the surface layer (0-5 cm) is used.

2.3.3 GLDAS Noah soil moisture product

The GLDAS dataset is produced by the LDAS (Land Data Assimilation System, https://ldas.gsfc.nasa.gov/gldas) that aims at providing spatial fields of land surface states (e.g. SMST) and fluxes (e.g. evapotranspiration and runoff) by integrating remote sensing and *in situ* observations based on advanced LSMs and data assimilation techniques (Rodell et al., 2004). Version 3.3 of Noah LSM is used to

https://doi.org/10.5194/essd-2020-209
Preprint. Discussion started: 16 October 2020

produce the GLDAS Noah product that is currently available from 2000 to the present at 3-hourly time interval with a spatial resolution of 0.25°. In this study, the data of soil water content for the top soil layer (0-10 cm) is used.

3 Methods

3.1 Spatial upscaling of soil moisture measurements

The principle of spatial upscaling method is to determine the weight for each SM monitoring site with the aid of extra information. The method generally follows the linear functional form, which can be mathematically defined as:

$$\overline{\boldsymbol{\theta}}_t^{ups} = \boldsymbol{\theta}_t^{obs}\boldsymbol{\beta} \tag{1a}$$

$$\boldsymbol{\theta}_t^{obs} = [\boldsymbol{\theta}_{t,1}^{obs}, \boldsymbol{\theta}_{t,2}^{obs}, \dots, \boldsymbol{\theta}_{t,N}^{obs}]^{\boldsymbol{T}} \tag{1b}$$

where $\overline{\boldsymbol{\theta}}_t^{ups}$[m^3 m^{-3}] represents the upscaled SM, $\boldsymbol{\theta}_t^{obs}$[m^3 m^{-3}] represents the vector of SM measurements, N represents the total number of SM monitoring sites, t represents the time (e.g. the t^{th} day), and β [-] represents the weight vector.

In this study, only the surface SM measurements taken from the Maqu and Shiquanhe networks are upscaled to obtain the regional-scale SM for a long-term period due to the availability of much longer data records in comparison to the Naqu and Ali networks (see Section 2.1). Four upscaling methods are investigated and inter-compared with each other to find the most suitable method for the application to the Tibet-Obs. Brief descriptions of the selected upscaling methods are given in Appendix A. The arithmetic averaging method (hereafter "AA") assigns an equal weight coefficient to each SM monitoring site (see Appendix A.1), while the Voronoi diagram method (hereafter "VD") determines the weight based on the geographic distribution of all the SM monitoring sites (see Appendix A.2). On the other hand, the time stability method (hereafter "TS") regards the most stable site as the representative site of the SM monitoring network (see Appendix A.3), while the apparent thermal inertia (ATI) method is based on the close relationship between apparent thermal inertia (τ) and SM (see Appendix A.4).

3.2 Trend analysis

As a nonparametric trend test, the Mann-Kendall (M-K) analysis (Mann, 1945) is widely used in hydrologic time series because it is not affected by the sample values and distribution types (Albergel et al., 2013; Burn & Hag Elnur, 2002). In this study, the M-K method is adopted to analyze the trend of upscaled SM time series (Section 3.1) and the model-based products (Section 2.2).

The tendency and significance of the trend are identified based on the calculation of the statistic UF_k [-] that is defined as:

$$UF_k = \frac{S_k - E(S_k)}{\sqrt{Var(S_k)}} \qquad k = 1, 2, \dots, n \tag{2a}$$

https://doi.org/10.5194/essd-2020-209
Preprint. Discussion started: 16 October 2020

where n represents the length of the average SM data, k represents the data order, S_k [-] is determined by the values of annual average SM (θ_i[m^3 m^{-3}]) compared with its subsequent data (θ_j [m^3 m^{-3}]) as given below:

$$S_k = \sum_{i=1}^{k} \sum_{j}^{i-1} \theta_{ij} \qquad k = 2, 3, \dots, n \tag{2b}$$

$$\theta_{ij} = \begin{cases} 1 & \theta_i > \theta_j \\ 0 & \theta_i < \theta_j \end{cases} \qquad 1 \leq \ j \leq i \tag{2c}$$

where i and j represent the data order. $E(S_k)$ and $Var(S_k)$ are the expectation and variance of S_k as given below:

$$\begin{cases} E(S_k) = \ k(k+1)/4 \\ Var(S_k) = k(k-1)(2k+5)/72 \end{cases} \tag{2d}$$

If the value of UF_k is positive, it indicates that the trend of the SM time series is upward, while the negative UF_k value implies a downtrend. The significance of the detected trend is obvious if the UF_kvalue is beyond the critical value that defined by a significant level (e.g. 0.05), otherwise, the tendency is considered to be not obvious. The mutation of the trend is identified by the intersection of UF_k and $UB_{k'}$ [-]. The statistic $UB_{k'}$ is calculated in the same way as the UF_k but in reverse chronological order as:

$$\begin{cases} UB_{k'} = \ -UF_k \\ k' = n + 1 - k \end{cases} \tag{2e}$$

3.3 Metrics used for statistical comparison

The metrics used to evaluate the accuracy of the upscaled SM are the bias (Bias [m^3 m^{-3}]), root-mean-square error (RMSE [m^3 m^{-3}]), and unbiased RMSE (ubRMSE [m^3 m^{-3}]) as:

$$\text{Bias} = \frac{\sum_{t=1}^{M} (\theta_t^{tru} - \boldsymbol{\bar{\theta}_t^{ups}})}{\text{M}} \tag{3a}$$

$$\text{RMSE} = \sqrt{\frac{\sum_{t=1}^{M} (\theta_t^{tru} - \boldsymbol{\bar{\theta}_t^{ups}})^2}{M}} \tag{3b}$$

$$\text{ubRMSE} = \sqrt{RMSE^2 - BIAS^2} \tag{3c}$$

where θ_t^{tru} represents the reference SM that is considered as the ground truth, and $\boldsymbol{\bar{\theta}_t^{ups}}$ represents the upscaled SM. The closer the metric is to zero, the more accurate the estimation is.

The metrics used for the correlation analysis are the Nash-Sutcliffe efficiency coefficient (NSE [-]) as:

$$\text{NSE} = 1 - \frac{\sum_{t=1}^{n} (\theta_t^{tru} - \boldsymbol{\bar{\theta}_t^{ups}})^2}{\sum_{t=1}^{n} (\theta_t^{tru} - \overline{\theta_t^{tru}})^2} \tag{4}$$

The value of the NSE ranges from -∞ to 1, and the closer the metric is to 1, the better the match of the estimated SM with the reference (θ_t^{tru}).

3.4 Preprocessing of model-based soil moisture products

The performance of the ERA5-land, MERRA2, and GLDAS Noah SM products are assessed using the upscaled SM data of the Maqu and Shiquanhe networks for a 10-year period. The corresponding regional-scale SM for each product can be obtained by averaging the grid data falling in the network areas. The numbers of grids covering the Maqu and Shiquanhe networks are 70 and 20 for the ERA5-land product, 12 and 4 for the GLDAS Noah product, and only one for the MERRA2 product. Moreover, the ERA5-land and

https://doi.org/10.5194/essd-2020-209
Preprint. Discussion started: 16 October 2020

MERRA2 products with the temporal resolution of hourly and 3-hourly are averaged to daily-scale, and the unit of GLDAS Noah SM is converted from kg m^{-2} to m^3 m^{-3}. The uppermost layer of the ERA5-land (0-7 cm), MERRA2 (0-5 cm), and GLDAS Noah SM products (0–10 cm) are considered to match the *in situ* observations at depth of 5 cm.

4 Results

4.1 Inter-comparison of soil moisture upscaling methods

In this section, four upscaling methods (see Section 3.1) are inter-compared first with the input of all the available SM monitoring sites for a single year in the Maqu and Shiquanhe networks to find the most suitable upscaled SM that can best represent the areal conditions. Later on, the performance of the four upscaling methods is further investigated with the input of different numbers of SM monitoring sites to find the most suitable method for producing long-term (~10 year) upscaled SM for the Maqu and Shiquanhe networks.

Fig. 2 shows the time series of daily average SM for the Maqu and Shiquanhe networks produced by the four upscaling methods based on the maximum number of available SM monitoring sites (hereafter "$SM_{AA\text{-}max}$", "$SM_{VD\text{-}max}$", "$SM_{TS\text{-}max}$", and "$SM_{ATI\text{-}max}$"). Two different periods are selected for the two networks due to the fact that the number of available sites reaches the maximum in different periods for the two network, e.g. 17 sites for Maqu between November 2009 and October 2010 and 12 sites for Shiquanhe between August 2018 and July 2019, respectively (see Tables A1 and A2 in the Appendix A). For the Maqu network, the $SM_{AA\text{-}max}$, $SM_{VD\text{-}max}$, and $SM_{TS\text{-}max}$ are comparable to each other, while the $SM_{ATI\text{-}max}$ shows distinct deviations during the winter (between December and February) and summer periods (between June and August). On the other hand, the $SM_{ATI\text{-}max}$ for the Shiquanhe network is comparable to $SM_{AA\text{-}max}$ and $SM_{VD\text{-}max}$, while deviation is observed for the $SM_{TS\text{-}max}$. It seems that the ATI method performs better in the Shiquanhe network due to the existence of a strong relationship between τ and θ in the desert ecosystem.

Table 6 lists the values of mean relative difference (*MRD*), standard deviation of the relative difference ($\sigma(RD)$), and comprehensive evaluation criterion (*CEC*) calculated for the upscaled SM produced by the four upscaling methods. The *CEC* (see Eq.(A6) in the Appendix A) is used here to determine the most suitable upscaled SM that can best represent the areal conditions for the two networks, and the *MRD* (Eq.(A4)) and $\sigma(RD)$ (Eq.(A3)) can be used to represent the bias and accuracy of the upscaled SM. It can be found that the $SM_{AA\text{-}max}$ yields the lowest *CEC* values for both networks, indicating that the $SM_{AA\text{-}max}$ can be used to represent actual areal conditions, which will thus be regarded as the ground truth for following analyses (hereafter "SM_{truth}").

As shown in Tables A1 and A2 (see Appendix A), the number of available SM monitoring sites decreases with increasing time span of *in situ* measurements. There are only three (i.e. CST05, NST01, and NST03) and four (i.e. SQ02, SQ03, SQ06, and SQ14) sites that provided more than nine years of *in situ* SM measurement data for the Maqu and Shiquanhe networks, respectively (see Tables 3 and 4). This indicates that the minimum number of available sites can be used to produce the long-term (~10 year) consistent

https://doi.org/10.5194/essd-2020-209
Preprint. Discussion started: 16 October 2020

upscaled SM are three and four for the Maqu and Shiquanhe networks, respectively. Fig. 3 shows the daily average SM time series produced by the four upscaling methods based on the minimum available monitoring sites (hereafter "AA-min", "TS-min", "VD-min", and "ATI-min"). The SM_{truth} obtained by the AA-max is also shown for comparison purpose. For the Maqu network, the upscaled SM produced by the AA-min, VD-min, and TS-min generally capture well the SM_{truth} variations, while the upscaled SM of the ATI-min shows dramatic deviations. Similarly, the upscaled SM produced by the AA-min and VD-min are consistent with the SM_{truth} for the Shiquanhe network with slight overestimations, while significant deviations are noted for the upscaled SM of the TS-min and ATI-min. Table 7 lists the error statistics (e.g. Bias, RMSE, ubRMSE, and NSE) computed between the upscaled SM produced by these four upscaling methods with the input of minimum available sites and the SM_{truth}. The upscaled SM produced by the AA-min shows better performance for both networks as indicated by the lower RMSE and higher NSE values in comparison to the other three upscaling methods.

Apart from the maximum and minimum numbers of available SM monitoring sites mentioned above, there are about 14, 10, 8, and 6 available sites during different time spans for the Maqu network, and for the Shiquanhe network are about 11, 10, 6 and 5 available sites (see Tables A1 and A2 in the Appendix A). Fig. 4 shows the bar chart of error statistics (i.e. RMSE and NSE) computed between the SM_{truth} and the upscaled SM produced by the four upscaling methods based on the input of different number of available sites. For the Maqu network, the performances of the AA and VD methods are better than the TS and ATI methods as indicated by smaller RMSEs and higher NSEs for all the estimations. A similar conclusion can be obtained for the Shiquanhe network, while the performance of the ATI method is largely improved when the number of available sites is not less than 10. It is interesting to note that the upscaled SM produced by the AA-min are comparable to those produced with more available sites (e.g. 10 sites) as indicated by comparable RMSE and NSE values for both networks. It indicates that the AA-min is suitable to produce long-term (~10 years) upscaled SM for both networks, which yield RMSEs of 0.022 and 0.011 $m^3\ m^{-3}$ for the Maqu and Shiquanhe networks in comparison to the SM_{truth} produced by the AA-max based on the maximum available sites.

4.2 Long-term analysis of upscaled soil moisture measurements

In this section, the AA-min is first adopted to produce the consecutive upscaled SM time series (hereafter "$SM_{AA\text{-}min}$") for an approximately 10-year period for the Maqu and Shiquanhe networks, respectively. In addition, the other time series of upscaled SM are produced by the AA method with input of all available SM monitoring sites regardless of the continuity (hereafter "$SM_{AA\text{-}valid}$"), which is widely used to validate the various SM products (Dente et al. 2012a; Chen et al. 2013; Zheng et al. 2018b) for a short term period (e.g. ≤ 2 years). This method may, however, leads to inconsistent SM time series for a long-term period due to the fact that the number of available sites is different in distinct periods (see Tables A1 and A2 in the Appendix A).

Fig. 5a shows the time series of $SM_{AA\text{-}min}$ and $SM_{AA\text{-}valid}$ along with the daily precipitation data for the Maqu network during the period between May 2009 and May 2019. Both two time series of the SM show similar

https://doi.org/10.5194/essd-2020-209
Preprint. Discussion started: 16 October 2020

seasonality with low values in winter due to frozen of soil and high values in summer due to rainfall. Deviations can be observed between the $SM_{AA\text{-}min}$ and $SM_{AA\text{-}valid}$ especially for the period between 2014 and 2019, whereby the $SM_{AA\text{-}valid}$ tends to produce smaller SM values in the warm season. Figs. 5b-5d show further the trends of the $SM_{AA\text{-}min}$, $SM_{AA\text{-}valid}$, and precipitation for a 10-year period produced by the M-K analysis method, respectively. As described in Section 3.2, the statistics *UF* and associated critical values, e.g. $UF_{0.05} = \pm 1.96$, can be used to indicate the tendency and significance of the detected trend, and the intersection of the *UF* and *UB* determines the mutation node. It can be found that both $SM_{AA\text{-}min}$ and $SM_{AA\text{-}valid}$ demonstrate a drying trend ($UF < 0$) that generally follows the trend of precipitation change for the entire period. Difference can be observed between the trends of $SM_{AA\text{-}min}$ and $SM_{AA\text{-}valid}$, whereby a significant drying trend is found for the $SM_{AA\text{-}valid}$ since 2014 due to the change of available SM monitoring sites (see Table A1). Specifically, several sites (e.g. NST11- NST15) located in the wetter area were damaged since 2013, and four new sites (i.e. NST21- NST25) were installed in the drier area in 2015 (see Table 3) that affect the trend of the $SM_{AA\text{-}valid}$.

Fig. 6a shows the time series of the $SM_{AA\text{-}min}$ and $SM_{AA\text{-}valid}$ along with the daily precipitation data for the Shiquanhe network during the period between August 2010 and August 2019. Both time series of the SM show similar seasonal variations as the Maqu network. However, obvious deviation can be noted for the inter-annual variations, and the $SM_{AA\text{-}valid}$ tends to produce lager values before 2014 but smaller values since then. Figs. 6b-6d show further the trends of the $SM_{AA\text{-}min}$, $SM_{AA\text{-}valid}$, and precipitation, respectively. The $SM_{AA\text{-}min}$ demonstrates a wetting trend ($UF > 0$) that generally follows the trend of precipitation change, while an opposite tendency is found for the $SM_{AA\text{-}valid}$ due to the change of available SM monitoring sites in distinct year (see Table A2). Specifically, several sites (e.g. SQ11 and SQ12) located in the wetter area were damaged around 2014, and five new sites (i.e. SQ17-21) were installed in the drier area in 2016.

In summary, the trends of the $SM_{AA\text{-}min}$ generally follow the trends of precipitation for both networks, while an opposite tendency is found for the $SM_{AA\text{-}valid}$ in the Shiquanhe network. The $SM_{AA\text{-}valid}$ are likely affected by the change of available SM monitoring sites over time that leads to inconsistent time series of SM. This indicates that the $SM_{AA\text{-}min}$ is superior to the $SM_{AA\text{-}valid}$ for the production of the long-term consistent upscaled SM time series. A drying trend is noted for the Maqu network due to weakening of monsoon that reduces the precipitation in the eastern part of TP, while a wetting trend is found for the Shiquanhe network due to the warming and moistening of atmosphere that leads to increasing convective rainfall in the western part of the TP (Yang et al., 2014).

4.3 Application of the long-term upscaled soil moisture to validate the model-based products

In this subsection, the long-term upscaled SM time series (i.e. $SM_{AA\text{-}min}$) produced for the two networks are applied to validate the reliability of three model-based SM products, i.e. ERA5-land, MERRA2, and GLDAS Noah. Since the ERA5-land only provides the data of volumetric total soil water content, the period when the soil is subject to freezing and thawing transition (i.e. November-April) is excluded for this evaluation.

https://doi.org/10.5194/essd-2020-209
Preprint. Discussion started: 16 October 2020

Fig. 7a shows the time series of $SM_{AA\text{-}min}$ and daily average SM data derived from the three products for the Maqu network during the period between May 2009 and May 2019. The error statistics, i.e. bias and RMSE, computed between the three products and the $SM_{AA\text{-}min}$ for both warm (May-October) and cold seasons (November-April) are given in Table 8. Although the three products generally capture the seasonal variations of the $SM_{AA\text{-}min}$, the magnitude of the temporal SM variability is underestimated. Both GLDAS Noah and MERRA2 products underestimate the SM measurements during the warm season leading to bias of about -0.112 and -0.113 $m^3\ m^{-3}$, respectively. This may be due to the fact that the LSMs adopted for producing these products do not consider the impact of vertical soil heterogeneity caused by organic matter contents widely existed in the surface layer of the Tibetan soil (Chen et al., 2013; Zheng et al., 2015a). In addition, the MERRA2 product overestimates the SM measurements during the cold season with bias of about 0.006 $m^3\ m^{-3}$. The ERA5-land product is able to capture the magnitude of $SM_{AA\text{-}min}$ dynamics in the warm season but with more fluctuation that yields a RMSE of about 0.067 $m^3\ m^{-3}$. The trends of the SM derived from the $SM_{AA\text{-}min}$ and the three products for the warm and cold seasons are shown in Fig. A1 (see Appendix A). Both the GLDAS Noah and MERRA2 products cannot reproduce the tendency and mutation node of the $SM_{AA\text{-}min}$ for both warm and cold seasons, and an opposite trend is noted for the GLDAS Noah product in cold season. The ERA5-land product is able to capture the trend of the $SM_{AA\text{-}min}$ but with higher significance of drying trend in the warm season.

Fig. 7b shows the time series of $SM_{AA\text{-}min}$ and daily SM data derived from the three products for the Shiquanhe network during the period between August 2010 and August 2018, and the corresponding error statistics are given in Table 8 as well. Although the three products generally capture the seasonal variations of the $SM_{AA\text{-}min}$, both GLDAS Noah and MERRA2 products overestimate the $SM_{AA\text{-}min}$ for the entire study period leading to positive bias values, and overestimation is also noted for the ERA5-land product in the warm season with bias of about 0.002 $m^3\ m^{-3}$.The trends of the SM derived from the $SM_{AA\text{-}min}$ and the three products for the warm and cold seasons are shown in Fig. A2 (see Appendix A). For the warm season, it is observed that both MERRA2 and ERA5-land products are able to reproduce the wetting trend of the $SM_{AA\text{-}min}$, while an opposite drying trend is noted for the GLDAS Noah product since 2015. For the cold season, the MERRA2 product also shows a comparable tendency with the $SM_{AA\text{-}min}$, while the GLDAS Noah product shows an opposite trend.

In summary, the currently model-based SM products still show deficiencies in representing the trend and variation of measured SM dynamics for a long-term period (~10 years) in the Tibetan grassland and desert ecosystems that dominate the landscape of the TP.

5 Discussion

As shown in previous sections, the number of available SM monitoring sites in the Tibet-Obs generally change with time, and there are not more than four sites providing more than 9 years of SM measurements for each network. The arithmetic average of all the available sites in each year leads to inconsistent time series of SM (i.e. $SM_{AA\text{-}valid}$, Section 4.2), while only utilizing the sites with long-term continuous

https://doi.org/10.5194/essd-2020-209
Preprint. Discussion started: 16 October 2020

measurements also shows biases, i.e. with RMSEs of 0.022 and 0.011 m^3 m^{-3} for the Maqu and Shiquanhe networks (Section 4.1). Therefore, it is necessary to find an appropriate strategy to maintain the Tibet-Obs for providing high-quality and long-term continuous SM measurements for the future. This section discusses the possible strategies for the Maqu and Shiquanhe networks as examples.

The impact of the number of available SM monitoring sites on the estimation of regional average SM is first quantified. A sensitivity analysis is conducted by changing the number of combined sites from 1 to maximum-1 using the random sampling method, and the time series of SM measurements described in Section 4.1 are adopted for the analysis (hereafter "control period"). The uncertainty of each combination is quantified by calculating the RMSE between the estimation of regional average SM and the SM_{truth}, which can be used to determine the number of monitoring sites required to achieve a specified uncertainty (Famiglietti et al., 2008; Zhao et al., 2013). Nine levels of RMSE standard are defined ranging from 0.004 to 0.02 m^3 m^{-3} at first, then the percentage of each combination's RMSE falling into different RMSE levels is computed as shown in Table 9. In general, the percentage increases with increasing number of available sites at any defined RMSE levels, which decreases when increasing the level of defined RMSE standard from 0.02 to 0.004 m^3 m^{-3}. If the RMSE standard is set as 0.004 m^3 m^{-3}, it is suggested to keep 16 and 11 sites for the Maqu and Shiquanhe networks to get a chance of more than 50 % to achieve the defined standard. The required number of sites decreases when lowering the RMSE standard to 0.01 m^3 m^{-3}, whereby 13 and 6 sites are recommended to get a chance of about 60 % for satisfying the defined standard. For the RMSE standard of 0.02 m^3 m^{-3}, it is suggested to keep 7 and 3 sites to get a chance of more than 50 % to achieve the defined standard. In summary, the number of available sites required to maintain current networks depends on the defined RMSE standard.

As shown in Section 4.1, the usage of a minimum number of sites with about 10-year continuous measurements yields RMSEs of 0.022 and 0.011 m^3 m^{-3} for the Maqu and Shiquanhe networks. In other words, it is suggested to maintain well the three (i.e. CST05, NST01, and NST03) and four (i.e. SQ02, SQ03, SQ06, and SQ14) monitoring sites for the Maqu and Shiquanhe networks if the RMSE standard are set as 0.022 and 0.011 m^3 m^{-3}, respectively. Since there are still 12 sites providing SM measurements for both networks until 2019 (see Tables 3 and 4), it is possible to decrease the RMSE values if the sites selected for maintaining are appropriately determined. For the Shiquanhe network, the optimal strategy is to keep the current 12 sites, which is exactly the combination used in Section 4.1. For the Maqu network, as shown in Table 9, the best level of RMSE can reach to 0.006 m^3 m^{-3} with the chance of 3.52 % for the combination of 12 sites. In order to find the optimal combination of the 12 sites for the Maqu network, all the possible combinations (i.e. C_{17}^{12} = 6188) are ranked through RMSE values from the smallest to largest. Table 10 lists the ranking 1-5 and 96-100 combinations, and it can be found that the 100th combination includes the maximum number of currently available sites (i.e. 7 sites including CST03, CST05, NST01, NST03, NST05, NST06, and NST10) with a RMSE of less than 0.006 m^3 m^{-3}. Therefore, the 100th combination of monitoring sites is suggested for the Maqu network.

https://doi.org/10.5194/essd-2020-209
Preprint. Discussion started: 16 October 2020

Open Access Earth System Science Data Discussions

In summary, it is suggested to maintain well current 12 sites for the Shiquanhe network, while for the Maqu network it is suggested to restore five old sites, i.e. CST02, NST11, NST13, NST14, and NST15.

6 Data availability

The 10-year (2009-2019) surface SM dataset is freely available from the 4TU.ResearchData repository at https://doi.org/10.4121/uuid:21220b23-ff36-4ca9-a08f-ccd53782e834 (Zhang et al., 2020). The original *in situ* and upscaled SM data is stored in .xlsx files. A user information file is given to introduce the content of these files and provide the download linkage of existing data and script used in this paper.

7 Conclusions

In this paper, we report on the status of the Tibet-Obs and present the long-term *in situ* SM and spatially upscaled SM dataset for the period 2009-2019. In general, the number of available SM monitoring sites decreased over time due to damage of sensors. Until 2019, there are only three and four sites that provide an approximately 10-year consistent SM measurements for the Maqu and Shiquanhe networks, respectively. Comparisons between four upscaling methods, i.e. arithmetic averaging (AA), Voronoi diagram (VD), time stability (TS) and apparent thermal inertia (ATI), show that the AA method with input of maximum number of available SM monitoring sites (AA-max) can be used to represent the actual areal SM conditions (SM_{truth}). The arithmetic average of the three and four sites with long-term continuous measurements (AA-min) are found to be most suitable to produce the upscaled SM dataset for the period 2009-2019, which may yield RMSEs of 0.022 and 0.011 m^3 m^{-3} for the Maqu and Shiquanhe networks in comparison to the SM_{truth}. Trend analysis of the approximately 10-year upsclaed SM datasets produced by the AA-min ($SM_{AA\text{-}min}$) shows that the Maqu area in the eastern part of TP is drying while the Shiquanhe area in the west is getting wet that generally follow the change of precipitation. The usage of all the available sites in each year leads to inconsistent time series of SM that cannot capture well the trend of precipitation changes. Comparisons between the $SM_{AA\text{-}min}$ and the model-based SM derived from the GLDAS Noah, MERRA2, and ERA5-land products further demonstrate that current model-based SM products still show deficiencies in representing the trend and variation of measured SM dynamics on the TP. Moreover, strategies for maintaining the Tibet-Obs are provided, and it is suggested to maintain well current 12 sites for the Shiquanhe network, while for the Maqu network it is suggested to restore five old sites.

The 10-year (2009-2019) surface SM dataset presented in this paper includes the 15-min *in situ* measurements taken at a depth of 5 cm collected from three regional-scale networks (i.e. Maqu, Naqu, and Ngari including Ali and Shiquanhe) of the Tibet-Obs, and the spatially upscaled SM datasets produced by the AA-min for the Maqu and Shiquanhe networks. This dataset is valuable for calibrating/validating long-term satellite- and model-based SM products, evaluation of SM upscaling methods, development of data fusion methods, and quantifying the coupling strength between precipitation and SM at 10-year scale.

Author contribution

Pei Zhang, Donghai Zheng, Rogier van der Velde and Zhongbo Su designed the framework of this work. Pei Zhang performed the computations and data analysis, and written the manuscript. Donghai Zheng, Rogier van der Velde and Zhongbo Su supervised the progress of this work and provided critical suggestions, and revised the manuscript. Zhongbo Su and Jun Wen designed the setup of Tibet-Obs, Yijian Zeng, XinWang and Zuoliang Wang involved in maintaining the Tibet-Obs and downloading the original measurements. Pei Zhang, Zuoliang Wang, and Jiali Chen organized the data.

Competing interests

The authors declare that they have no conflict of interest.

Acknowledgments

This study was supported by the Strategic Priority Research Program of Chinese Academy of Sciences (Grant No. XDA20100103) and National Natural Science Foundation of China (Grant No. 41971308，41871273).

Reference

Albergel, C., Dorigo, W., Reichle, R. H., Balsamo, G., Derosnay, P., Muñoz-sabater, J., Isaksen, L., Dejeu, R. and Wagner, W.: Skill and global trend analysis of soil moisture from reanalyses and microwave remote sensing, Journal of Hydrometeorology, 14(4), 1259–1277, doi:10.1175/JHM-D-12-0161.1, 2013.

Albergel, C., Dutra, E., Munier, S., Calvet, J.-C., Muñoz Sabater, J., Rosnay, P. and Balsamo, G.: ERA-5 and ERA-Interim driven ISBA land surface model simulations: Which one performs better?, Hydrology and Earth System Sciences, 22, doi:10.5194/hess-22-3515-2018, 2018.

Bi, H. and Ma, J.: Evaluation of simulated soil moisture in GLDAS using in-situ measurements over the Tibetan Plateau, International Geoscience and Remote Sensing Symposium (IGARSS), 2015-Novem, 4825–4828, doi:10.1109/IGARSS.2015.7326910, 2015.

Burn, D. H. and Hag Elnur, M. A.: Detection of hydrologic trends and variability, Journal of Hydrology, 255(1–4), 107–122, doi:10.1016/S0022-1694(01)00514-5, 2002.

Chen, Y., Yang, K., Qin, J., Zhao, L., Tang, W. and Han, M.: Evaluation of AMSR-E retrievals and GLDAS simulations against observations of a soil moisture network on the central Tibetan Plateau, Journal of Geophysical Research Atmospheres, 118(10), 4466–4475, doi:10.1002/jgrd.50301, 2013.

Cheng, M., Zhong, L., Ma, Y., Zou, M., Ge, N., Wang, X. and Hu, Y.: A study on the assessment of multi-source satellite soil moisture products and reanalysis data for the Tibetan Plateau, Remote Sensing, 11(10), doi:10.3390/rs11101196, 2019.

Colliander, A., Jackson, T. J., Bindlish, R., Chan, S., Das, N., Kim, S. B., Cosh, M. H., Dunbar, R. S., Dang, L., Pashaian, L., Asanuma, J., Aida, K., Berg, A., Rowlandson, T., Bosch, D., Caldwell, T., Caylor, K., Goodrich, D., al Jassar, H., Lopez-Baeza, E., Martínez-Fernández, J., González-Zamora, A., Livingston, S., McNairn, H., Pacheco, A., Moghaddam, M., Montzka, C., Notarnicola, C., Niedrist, G., Pellarin, T., Prueger, J., Pulliainen, J., Rautiainen, K., Ramos, J., Seyfried, M., Starks, P., Su, Z., Zeng, Y., van der Velde, R., Thibeault, M., Dorigo, W., Vreugdenhil, M., Walker, J. P., Wu, X., Monerris, A., O'Neill, P. E., Entekhabi, D., Njoku, E. G. and Yueh, S.: Validation of SMAP surface soil moisture products with core validation sites, Remote Sensing of Environment, 191, 215–231, doi:10.1016/j.rse.2017.01.021, 2017.

Dente, L., Vekerdy, Z., Wen, J. and Su, Z.: Maqu network for validation of satellite-derived soil moisture products, International Journal of Applied Earth Observation and Geoinformation, 17, 55–65, doi.org/10.1016/j.jag.2011.11.004, 2012a.

Dente, L., Su, Z. and Wen, J.: Validation of SMOS soil moisture products over the Maqu and Twente Regions, Sensors (Switzerland), 12(8), 9965–9986, doi:10.3390/s120809965, 2012b.

Van doninck, J., Peters, J., De Baets, B., De Clercq, E. M., Ducheyne, E. and Verhoest, N. E. C.: The potential of multitemporal Aqua and Terra MODIS apparent thermal inertia as a soil moisture indicator, International Journal of Applied Earth Observation and Geoinformation, 13(6), 934–941, doi.org/10.1016/j.jag.2011.07.003, 2011.

Famiglietti, J. S., Ryu, D., Berg, A. A., Rodell, M. and Jackson, T. J.: Field observations of soil moisture variability across scales, Water Resources Research, 44(1), 1–16, doi:10.1029/2006WR005804, 2008.

Gelaro, R., McCarty, W., Suárez, M. J., Todling, R., Molod, A., Takacs, L., Randles, C., Darmenov, A., Bosilovich, M. G., Reichle, R., Wargan, K., Coy, L., Cullather, R., Draper, C., Akella, S., Buchard, V., Conaty, A., da Silva, A., Gu, W., Kim, G.-K., Koster, R., Lucchesi, R., Merkova, D., Nielsen, J. E., Partyka, G., Pawson, S., Putman, W., Rienecker, M., Schubert, S. D., Sienkiewicz, M. and Zhao, B.: The Modern-Era Retrospective Analysis for Research and Applications, Version 2 (MERRA-2), Journal of climate, Volume 30(Iss 13), 5419–5454, doi:10.1175/JCLI-D-16-0758.1, 2017.

Muñoz-Sabater, J., Dutra E., Balsamo G., B. S., E., Z., C., A. and A., and A.-P.: ERA5-Land: an improved version of the ERA5 reanalysis land component, Joint ISWG and LSA-SAF Workshop IPMA, Lisbon, 26–28, 2018.

Jacobs, J. M., Mohanty, B. P., Hsu, E.-C. and Miller, D.: SMEX02: Field scale variability, time stability and similarity of soil moisture, Remote Sensing of Environment, 92(4), 436–446, doi:https://doi.org/10.1016/j.rse.2004.02.017, 2004.

Ju, F., An, R. and Sun, Y.: Immune evolution particle filter for soil moisture data assimilation, Water (Switzerland), 11(2), doi:10.3390/w11020211, 2019.

Kang, J., Jin, R., Li, X. and Zhang, Y.: Block Kriging With Measurement Errors: A Case Study of the Spatial Prediction of Soil Moisture in the Middle Reaches of Heihe River Basin, IEEE Geoscience and

Remote Sensing Letters, 14(1), 87–91, doi:10.1109/LGRS.2016.2628767, 2017.

Li, C., Lu, H., Yang, K., Han, M., Wright, J. S., Chen, Y., Yu, L., Xu, S., Huang, X. and Gong, W.: The evaluation of SMAP enhanced soil moisture products using high-resolution model simulations and in-situ observations on the Tibetan Plateau, Remote Sensing, 10(4), 1–16, doi:10.3390/rs10040535, 2018.

Liu, J., Chai, L., Lu, Z., Liu, S., Qu, Y., Geng, D., Song, Y., Guan, Y., Guo, Z., Wang, J. and Zhu, Z.: Evaluation of SMAP, SMOS-IC, FY3B, JAXA, and LPRM Soil moisture products over the Qinghai-Tibet Plateau and Its surrounding areas, Remote Sensing, 11(7), doi:10.3390/rs11070792, 2019.

Mann, H. B.: Nonparametric Tests Against Trend, Econometrica, 13(3), 245–259, doi:10.2307/1907187, 1945.

Qin, J., Yang, K., Lu, N., Chen, Y., Zhao, L. and Han, M.: Spatial upscaling of in-situ soil moisture measurements based on MODIS-derived apparent thermal inertia, Remote Sensing of Environment, 138, 1–9, doi:10.1016/j.rse.2013.07.003, 2013.

Qin, J., Zhao, L., Chen, Y., Yang, K., Yang, Y., Chen, Z. and Lu, H.: Inter-comparison of spatial upscaling methods for evaluation of satellite-based soil moisture, Journal of Hydrology, 523, 170–178, doi:10.1016/j.jhydrol.2015.01.061, 2015.

Rodell, M., Houser, P. R., Jambor, U., Gottschalck, J., Mitchell, K., Meng, C.-J., Arsenault, K., Cosgrove, B., Radakovich, J., Bosilovich, M., Entin, J. K., Walker, J. P., Lohmann, D. and Toll, D.: The Global Land Data Assimilation System, Bulletin of the American Meteorological Society, 85(3), 381–394, doi:10.1175/BAMS-85-3-381, 2004.

Su, Z., Wen, J., Dente, L., Van Der Velde, R., Wang, L., Ma, Y., Yang, K. and Hu, Z.: The tibetan plateau observatory of plateau scale soil moisture and soil temperature (Tibet-Obs) for quantifying uncertainties in coarse resolution satellite and model products, Hydrology and Earth System Sciences, 15(7), 2303–2316, doi:10.5194/hess-15-2303-2011, 2011.

Su, Z., De Rosnay, P., Wen, J., Wang, L. and Zeng, Y.: Evaluation of ECMWF's soil moisture analyses using observations on the Tibetan Plateau, Journal of Geophysical Research Atmospheres, 118(11), 5304–5318, doi:10.1002/jgrd.50468, 2013.

Tarantola, A.: Inverse Problem Theory and Methods for Model Parameter Estimation, Society for Industrial and Applied Mathematics., 2005.

Vachaud, G., Passerat De Silans, A., Balabanis, P. and Vauclin, M.: Temporal Stability of Spatially Measured Soil Water Probability Density Function1, Soil Science Society of America Journal, 49, 822–828, doi:10.2136/sssaj1985.03615995004900040006x, 1985.

van der Velde, R., Su, Z. and Wen, J.: Roughness determination from multi-angular ASAR Wide Swath mode observations for soil moisture retrieval over the Tibetan Plateau, Proceedings of the European Conference on Synthetic Aperture Radar, EUSAR, Proceeding(August 2011), 163–165, 2014.

Veroustraete, F., Li, Q., Verstraeten, W. W., Chen, X., Bao, A., Dong, Q., Liu, T. and Willems, P.: Soil

https://doi.org/10.5194/essd-2020-209
Preprint. Discussion started: 16 October 2020

moisture content retrieval based on apparent thermal inertia for Xinjiang province in China, International Journal of Remote Sensing, 33(12), 3870–3885, doi:10.1080/01431161.2011.636080, 2012.

Wei, Z., Meng, Y., Zhang, W., Peng, J. and Meng, L.: Downscaling SMAP soil moisture estimation with gradient boosting decision tree regression over the Tibetan Plateau, Remote Sensing of Environment, 225(February), 30–44, doi:10.1016/j.rse.2019.02.022, 2019.

Yang, K., Wu, H., Qin, J., Lin, C., Tang, W. and Chen, Y.: Recent climate changes over the Tibetan Plateau and their impacts on energy and water cycle: A review, Global and Planetary Change, 112, 79–91, doi:10.1016/j.gloplacha.2013.12.001, 2014.

Yang, K., Chen, Y., He, J., Zhao, L., Lu, H. and Qin, J.: Development of a daily soil moisture product for the period of 2002-2011 in Mainland China., Science China Earth Sciences, doi:10.1007/s11430-019-9588-5, 2020.

Zeng, J., Li, Z., Chen, Q., Bi, H., Qiu, J. and Zou, P.: Evaluation of remotely sensed and reanalysis soil moisture products over the Tibetan Plateau using in-situ observations, Remote Sensing of Environment, 163, 91–110, doi.org/10.1016/j.rse.2015.03.008, 2015.

Zeng, Y., Su, Z., Van Der Velde, R., Wang, L., Xu, K., Wang, X. and Wen, J.: Blending satellite observed, model simulated, and in situ measured soil moisture over Tibetan Plateau, Remote Sensing, 8(3), 1–22, doi:10.3390/rs8030268, 2016.

Zhang, P., Zheng, D., van der Velde, R., Wen, J., Zeng, Y., Wang, X., Wang, Z., Chen, J. and Su, Z.: A 10-year (2009-2019) surface soil moisture dataset produced based on in situ measurements collected from the Tibet-Obs. 4TU.ResearchData. Dataset. https://doi.org/10.4121/uuid:21220b23-ff36-4ca9-a08f-ccd53782e834, 2020.

Zhang, Q., Fan, K., Singh, V. P., Sun, P. and Shi, P.: Evaluation of Remotely Sensed and Reanalysis Soil Moisture Against In Situ Observations on the Himalayan-Tibetan Plateau, Journal of Geophysical Research: Atmospheres, 123(14), 7132–7148, doi:10.1029/2017JD027763, 2018.

Zhao, L., Yang, K., Qin, J., Chen, Y., Tang, W., Montzka, C., Wu, H., Lin, C., Han, M. and Vereecken, H.: Spatiotemporal analysis of soil moisture observations within a Tibetan mesoscale area and its implication to regional soil moisture measurements, Journal of Hydrology, 482, 92–104, doi:10.1016/j.jhydrol.2012.12.033, 2013.

Zhao, W., Li, A., Jin, H., Zhang, Z., Bian, J. and Yin, G.: Performance evaluation of the triangle-based empirical soil moisture relationship models based on Landsat-5 TM data and in situ measurements, IEEE Transactions on Geoscience and Remote Sensing, 55(5), 2632–2645, doi:10.1109/TGRS.2017.2649522, 2017.

Zheng, D., van der Velde, R., Su, Z., Wang, X., Wen, J., Booij, M. J., Hoekstra, A. Y. and Chen, Y.: Augmentations to the Noah Model Physics for Application to the Yellow River Source Area. Part I: Soil Water Flow, Journal of Hydrometeorology, 16(6), 2659–2676, doi:10.1175/JHM-D-14-0198.1, 2015a.

https://doi.org/10.5194/essd-2020-209
Preprint. Discussion started: 16 October 2020

Zheng, D., van der Velde, R., Su, Z., Wang, X., Wen, J., Booij, M. J., Hoekstra, A. Y. and Chen, Y.: Augmentations to the Noah Model Physics for Application to the Yellow River Source Area. Part II: Turbulent Heat Fluxes and Soil Heat Transport, Journal of Hydrometeorology, 16(6), 2677–2694, doi:10.1175/JHM-D-14-0199.1, 2015b.

Zheng, D., van der Velde, R., Wen, J., Wang, X., Ferrazzoli, P., Schwank, M., Colliander, A., Bindlish, R. and Su, Z.: Assessment of the SMAP Soil Emission Model and Soil Moisture Retrieval Algorithms for a Tibetan Desert Ecosystem, IEEE Transactions on Geoscience and Remote Sensing, 56(7), 3786–3799, doi:10.1109/TGRS.2018.2811318, 2018a.

Zheng, D., Wang, X., van der Velde, R., Ferrazzoli, P., Wen, J., Wang, Z., Schwank, M., Colliander, A., Bindlish, R. and Su, Z.: Impact of surface roughness, vegetation opacity and soil permittivity on L-band microwave emission and soil moisture retrieval in the third pole environment, Remote Sensing of Environment, 209(November 2017), 633–647, doi:10.1016/j.rse.2018.03.011, 2018b.

Zheng, D., Wang, X., van der Velde, R., Schwank, M., Ferrazzoli, P., Wen, J., Wang, Z., Colliander, A., Bindlish, R. and Su, Z.: Assessment of Soil Moisture SMAP Retrievals and ELBARA-III Measurements in a Tibetan Meadow Ecosystem, IEEE Geoscience and Remote Sensing Letters, 16(9), 1407–1411, doi:10.1109/lgrs.2019.

https://doi.org/10.5194/essd-2020-209
Preprint. Discussion started: 16 October 2020

Open Access Earth System Science Data Discussions

612 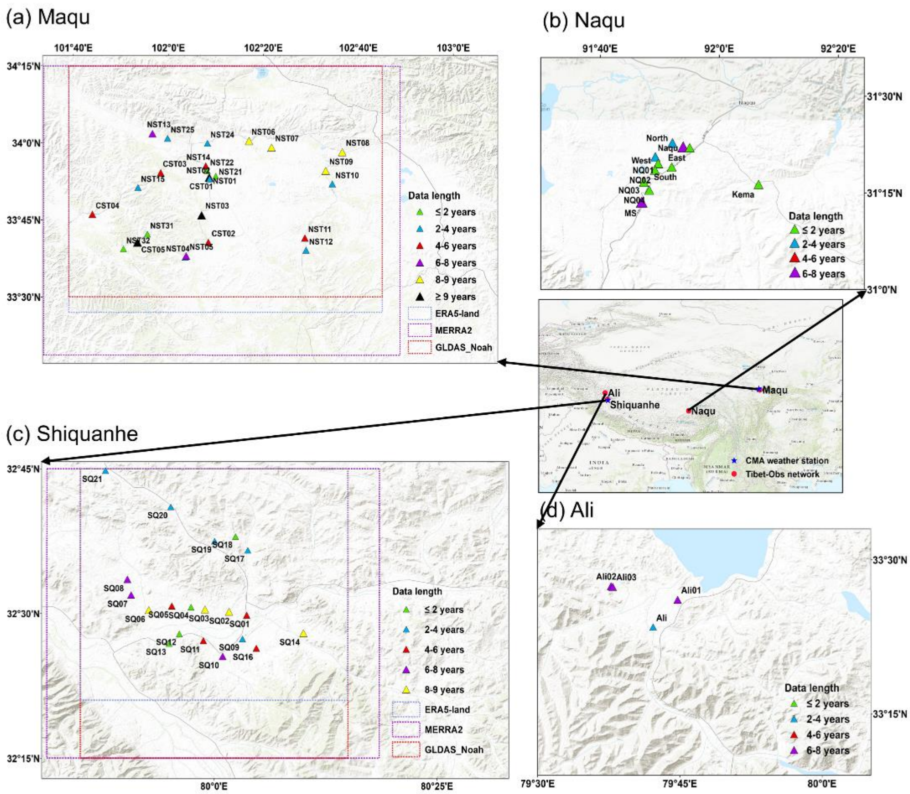

613 **Fig. 1. Locations of the Tibet-Obs: (a) Maqu, (b) Naqu, (c) Shiquanhe and (d) Ali SMST monitoring networks.**
614 **The colored triangles represent different data lengths of surface SM measurements for each site. The colored**
615 **boxes represent the coverage of selected model-based products. The weather stations of Maqu and Shiquanhe**
616 **operated by the China Meteorological Administration are also shown. (Base map from Esri, Copyright © Esri)**

617

618 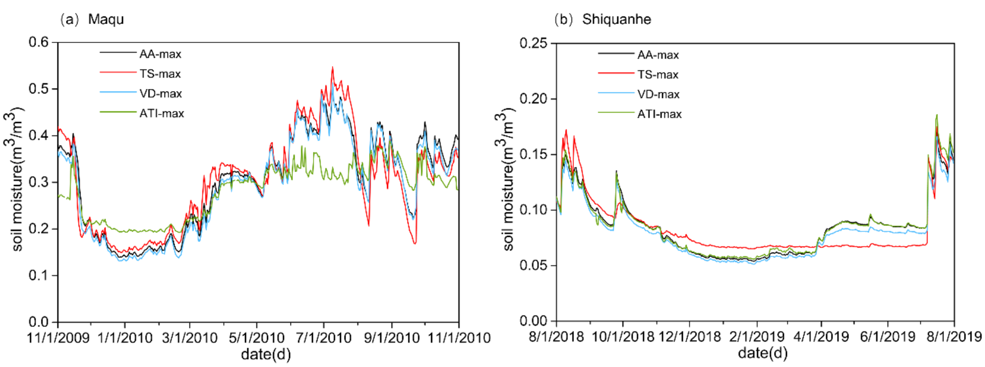

619 **Fig. 2. Comparisons of daily average SM for the (a) Maqu and (b) Shiquanhe networks produced by the four**
620 **upscaling methods with input of maximum number of available SM monitoring sites.**

https://doi.org/10.5194/essd-2020-209
Preprint. Discussion started: 16 October 2020

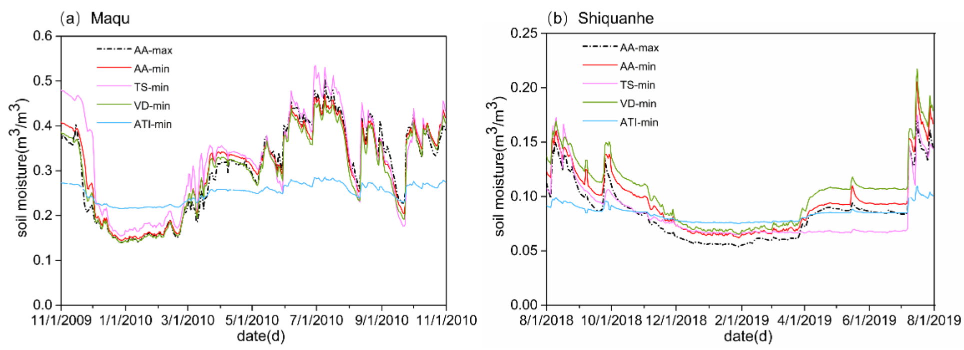

Fig. 3. Comparisons of daily average SM for the (a) Maqu and (b) Shiquanhe networks produced by the four upscaling methods with input of minimum number of available SM monitoring sites.

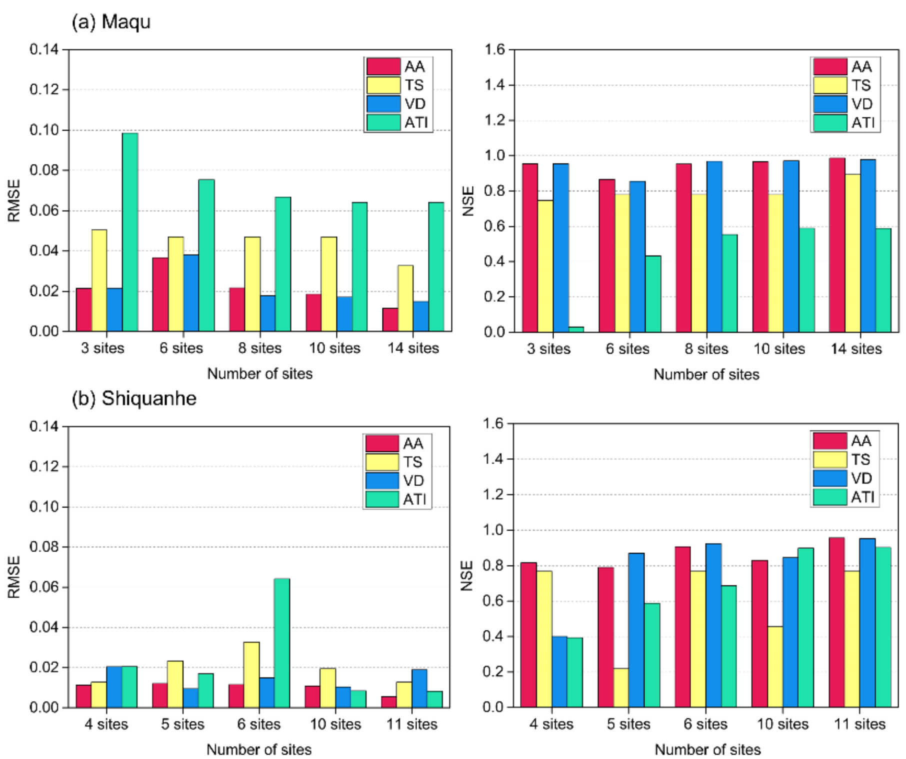

Fig. 4. Histograms of error statistics computed between the SM_{truth} produced by the AA-max and the upscaled SM produced by the four upscaling methods with input of different number of available SM monitoring sites for the (a) Maqu and (b) Shiquanhe networks.

https://doi.org/10.5194/essd-2020-209
Preprint. Discussion started: 16 October 2020

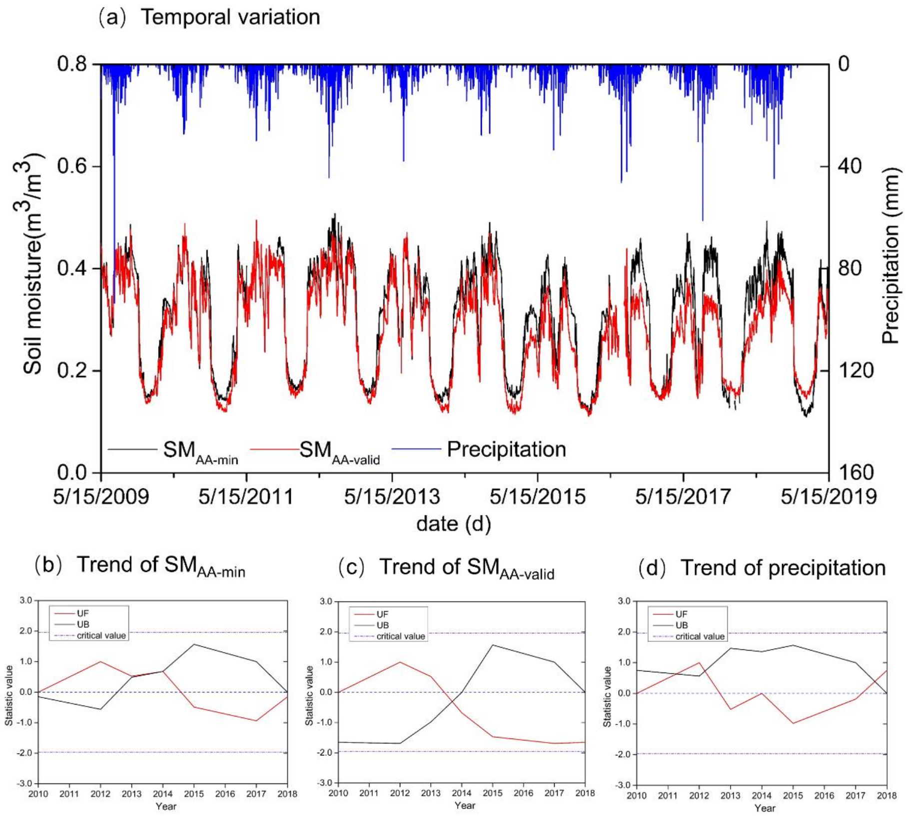

Fig. 5. (a) Temporal variation and trend of (b) SM$_{AA\text{-}min}$, (c) SM$_{AA\text{-}valid}$ and (d) precipitation for the Maqu network in a 10-year period.

https://doi.org/10.5194/essd-2020-209
Preprint. Discussion started: 16 October 2020

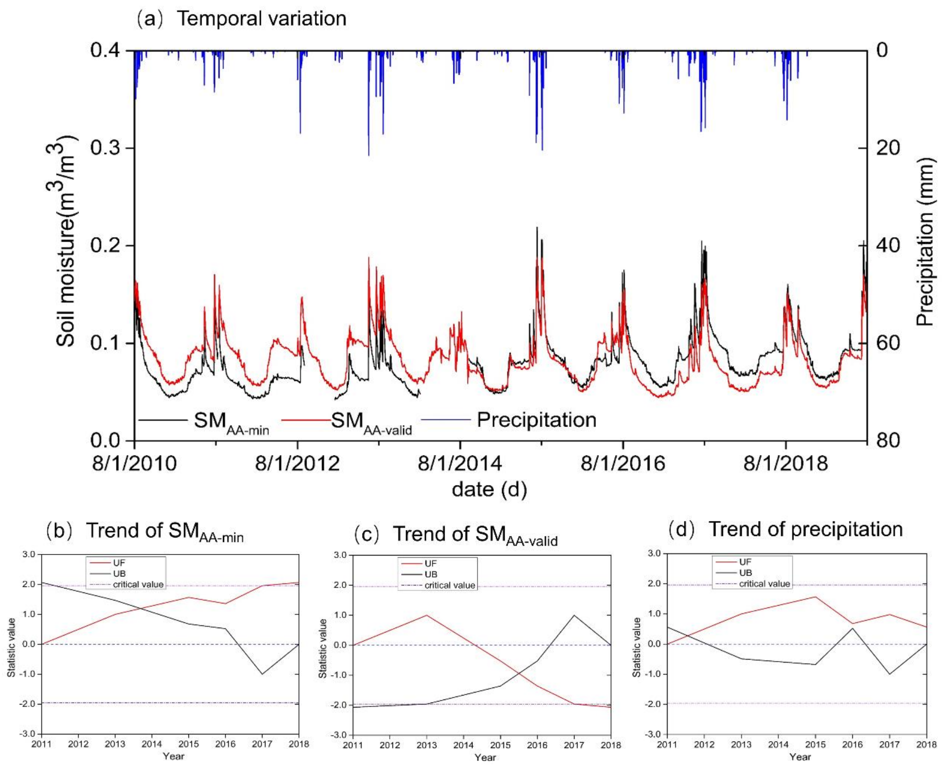

634

635 **Fig. 6. Same as Fig. 5 but for the Shiquanhe network.**

636

https://doi.org/10.5194/essd-2020-209
Preprint. Discussion started: 16 October 2020

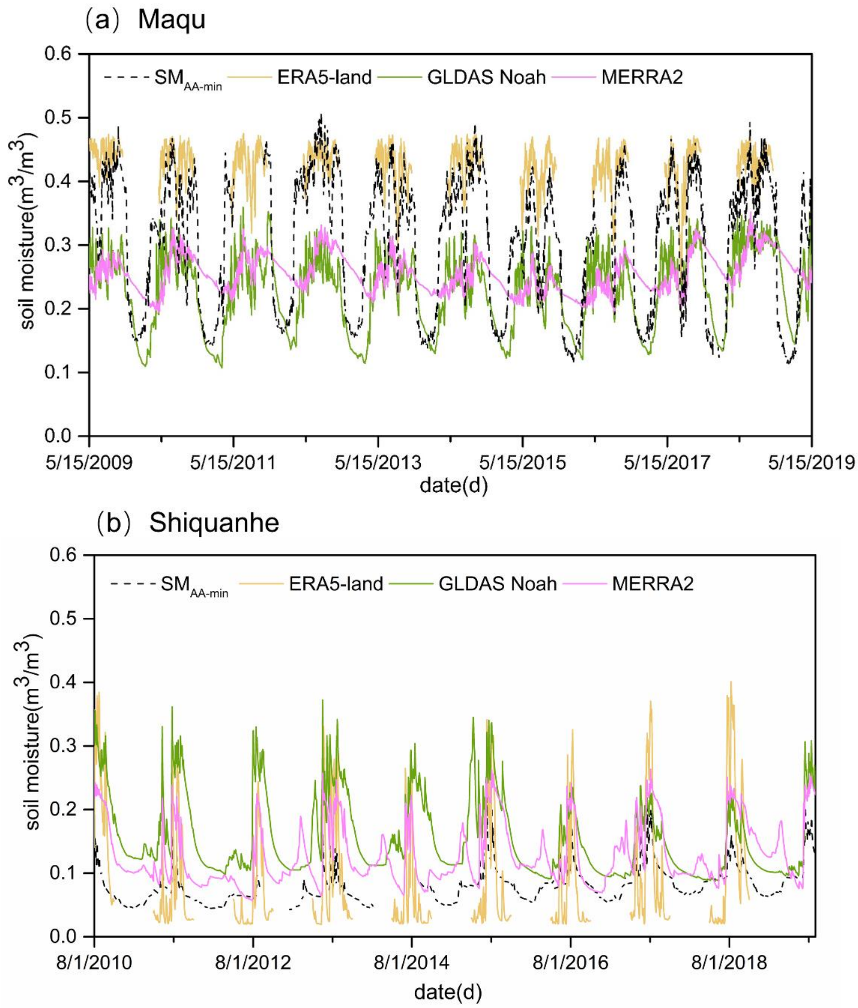

637

638 **Fig. 7. Comparisons between the model-based SM derived from the ERA5-land, MERRA2, and GLDAS Noah**
639 **products and the upscaled SM (SM_{AA-min}) for the (a) Maqu and (b) Shiquanhe networks in a 10-year period.**

640

641

https://doi.org/10.5194/essd-2020-209
Preprint. Discussion started: 16 October 2020

Table 1. Summary of the main Tibet-Obs applications and corresponding findings.

Literature	*In situ* data	Satellite- and/or model-based products	Key findings
Dente et al. (2012a)	Maqu network, period between 2008 and 2009	LPRM AMSR-E SM product, ASCAT SM product	i) The weighted average of SM depended on the percentage spatial coverage strata can be regarded as the ground reference. ii) The AMSR-E and ASCAT products are able to provide reasonable area SM during monsoon seasons.
Dente et al. (2012b)	Maqu network, period of 2010	Soil Moisture and Ocean Salinity (SMOS) Level 2 SM product	The SMOS product exhibits a systematic dry bias (0.13 m^3 m^{-3}) at the Maqu network.
Zeng et al. (2015)	Maqu network, period between 2008 and 2010	SMOS Level 3 SM product (version 2.45), Advanced Microwave Scanning Radiometer for Earth Observation System SM products (AMSR-E) SM products developed by National Aeronautics and Space Administration (NASA version 6), Land Parameter Retrieval Model (LPRM version 2), and Japan Aerospace Exploration Agency (JAXA version 700), AMSR2 Level 3 SM product (version 1.11), Advanced Scatterometer SM product (ASCAT version TU-Wien-WARP 5.5), ERA-Interim SM product (version 2.0), and Essential Climate Variable SM product (ECV version 02.0)	i) The ECV and ERA products give the best performance, and all products are able to capture the SM dynamic except for the NASA product. ii) The JAXA AMSR-E/AMSR2 products underestimate SM, while the ASCAT product overestimates it. iii) The SMOS product exhibits big noise and bias, and the LPRM AMSR-E product shows a significantly larger seasonal amplitude.
Zheng et al. (2015a)	Maqu network, period between 2009 and 2010	Noah LSM (land surface model) simulations	The modified hydraulic parameterization is able to resolve the SM underestimation in the upper soil layer under wet conditions, and it also leads to better capture for SM profile dynamics combined with the modified root distribution.
Bi & Ma (2015)	Maqu network, period between 2008 and 2011	GLDAS SM products produced by Noah, Mosaic CLM and Variable Infiltration Capacity (VIC) models	The SM simulated by the four LSMs can give reasonable SM dynamics but still show negative biases probably resulted from the high soil organic carbon content.
Li et al. (2018)	Maqu network, period between 2015 and 2016	Soil Moisture Active Passive (SMAP) Level 3 standard (36km) and enhanced (9km) passive SM products (version 3), Community Land Model (CLM4.5) simulations	i) The standard and enhanced SMAP products have similar performance for SM spatial distributions. ii) The SM of enhanced SMAP product exhibits good agreement with the CLM4.5 SM simulation.
Zhao et al. (2017)	Maqu network, period between 2008 and 2010	Downscaled SM from five typical triangle-based empirical SM relationship models	The model treating the surface SM as a second-order polynomial with LST, vegetation indices, and surface albedo outperforms other models.
Ju et al. (2019)	Maqu network, period of 2012	VIC LSM simulations	The IEPFM (immune evolution particle filter with Markov chain Monte Carlo simulation) is able to mitigate particle impoverishment and provide better assimilation results.
Zheng et al. (2018b)	Ngari network, period between 2015 and 2016	SMAP Level 2 radiometer SM product	Modifying surface roughness and employing soil temperature and texture information can improve the SMAP SM retrievals for the desert ecosystem of the TP.
Zhang et al. (2018)	Maqu and Ngari networks, period between 2010 and 2013	ERA-Interim SM product, MERRA SM product, GLDAS_Noah SM product (version2.0 and version2.1)	All these products exhibit overestimation at the Ngari network while underestimation at the Maqu network except for the ERA-Interim product.

https://doi.org/10.5194/essd-2020-209
Preprint. Discussion started: 16 October 2020

Zheng et al. (2018a)	Maqu and Ngari networks, period between 2015 and 2016	SMAP Level 1C radiometer brightness temperature products (version 3)	i) The SMAP algorithm underestimates the significance of surface roughness while overestimates the impact of vegetation. ii) The modified brightness temperature simulation can result in better SM retrievals.
Wei et al. (2019)	Maqu and Ngari networks, period between 2015 and 2016	SMAP Level 3 SM passive product	The downscaled SM still can keep accuracy compared to the SM of original SMAP product.
Liu et al. (2019)	Maqu and Ngari networks, period between 2012 and 2016	SMAP Level 3 SM products (version 4.00), SMOS-IC SM products (version 105), Fengyun-3B Microwave Radiation Image SM product (FY3B MWRI), JAXA AMSR2 Level 3 SM product, LPRM AMSR2 Level 3 SM product (version 3.00)	i) The JAXA AMSR2 product underestimates area SM while the LPRM AMSR2 product overestimates it. ii) The SMOS-IC product exhibits some noise of SM temporal variation. iii) The SMAP product has the highest accuracy among the five products while FY3B shows relatively lower accuracy.
Yang et al. (2020)	Maqu and Ngari network, period between 2008 and 2011	AMSR-E brightness temperature product	The assimilated SM products exhibit higher accuracy than the AMSR-E product and LSM simulations for wet areas, whereas their accuracy is similar for dry areas.
Su et al. (2013)	Maqu and Naqu networks, period between 2008 and 2009.	AMSR-E SM product, ASCAT Level 2 SM product, ECMWF SM analyses i.e. optimum interpolation and extended Kalman filter products	i) The Naqu area SM is overestimated by the ECMWF products in monsoon seasons, while the Maqu area SM produced by the ECMWF is comparable to previous studies. ii) The SM estimate cannot be considerably improved by assimilating ASCAT data due to the CDF matching approach and the data quality.
Zeng et al. (2016)	Maqu, Naqu and Ngari networks, period between 2010 and 2011	LPRM AMSR-E SM product, ERA-Interim SM product	The blended SM is able to capture temporal variations across different climatic zones over the TP.
Cheng et al. (2019)	Maqu, Naqu and Ngari networks, period of 2010	European Space Agency Climate Change Initiative Soil Moisture SM product (ESA CCISM version 4.4), ERA5 SM product	i) The seasonal variation and spatial distribution of SM can be captured by all four products i.e., ESA CCI_active, ESA CCI_passive, ESA CCI_combined, and ERA5. ii) The ESA CCI_active and ESA CCI_combined products exhibit narrower magnitude than the ESA CCI passive and ERA5 products. iii) The SM uptrend across the TP can be found from the ERA5 product.

https://doi.org/10.5194/essd-2020-209
Preprint. Discussion started: 16 October 2020

Table 2. Basic information of the Tibet-Obs.

Networks		Sites	Elevation (m)	Climate	Dominated land cover	Dominated soil texture
Maqu		28	3400-3800	Cold humid	Grassland	Silt loam
Ngari	Shiquanhe	21	4200-4700	Cold arid	Desert	Fine sand
	Ali	4	4250-4300			
Naqu		11	4500	Cold semiarid	Grassland	Loamy sand

Table 3. Data records of all the SMST monitoring sites performed for the Maqu network. Green shaded cells represent that there is not data missing, blue and pink shaded cells represent that the lengths of data missing are less than and more than one month for each year, respectively. Blank cells represent that there is not measurement performed. The number represents the month(s) when the data is missing.

	2009	2010	2011	2012	2013	2014	2015	2016	2017	2018	2019	Data length (months)
CST01			**10~12**	**1~6 10~12**								**36**
CST02			**5~12**	**1~10**	**6**	**7~12**						**46**
CST03					**6~12**	**1~10**	**7~12**			**1~9**	**5~12**	**68**
CST04	**1~5**		**12**	**1~3 11~12**	**1~2 6**	**8~10**	**7~12**		**1~6**	**7~12**		**73**
CST05					**6**			**5~7**		**1~2**	**6~12**	**119**
NST01	**1~5**				**6**			**5~7**			**6~12**	**116**
NST02	**1~3**			**7~8 10~12**								**40**
NST03			**5~10**		**6**			**5~7**			**6~12**	**115**
NST04			**10~12**									**33**
NST05	**3~5**				**6~12**	**1~7**		**5~7**	**7~12**	**1~7**	**6~12**	**92**
NST06		**1~3 12**	**1~3**		**6**			**6~7**	**8~12**	**1~7**	**6~12**	**104**
NST07			**3**		**6, 12**	**1**	**12**	**1~2 7,12**	**1~2 12**	**1~3 9~12**		**101**
NST08		**2, 4 9~12**	**1~5**		**6~10**	**1~10**		**6~7**			**6~12**	**95**
NST09	**1, 12**	**1~4 12**	**1~3**		**1~2 6**	**7~10**	**12**	**1~3 7, 12**	**1~2 7**		**6~12**	**99**
NST10		**11~12**	**1~5 7~12**	**1~6**	**6~12**					**1~7**	**6~12**	**44**
NST11				**7~8**	**6**	**7~12**						**63**
NST12	**10~12**	**1~9**			**6~12**	**1~10**	**7~12**					**49**
NST13					**6**		**7~12**					**77**
NST14	**6~9**				**6**	**10~12**						**64**
NST15		**10~12**	**1~5**	**6~12**								**33**
NST21						**1~7**	**7~12**					**11**

https://doi.org/10.5194/essd-2020-209
Preprint. Discussion started: 16 October 2020

Open Access Earth System Science Data Discussions

NST22						1~7	7~12					11
NST24						1~7	2~12	1~7			6~12	40
NST25						1~7		2~12	1~8		6~12	39
NST31									1~8	7~12		10
NST32										1~5	6~12	12

Table 4. Same as the Table 3 but for the Ngari network.

	2010	**2011**	**2012**	**2013**	**2014**	**2015**	**2016**	**2017**	**2018**	**2019**	**Data length (months)**
						Shiquanhe network					
SQ01	1~7				9~12	1~9					52
SQ02	1~7				5~9					9~12	104
SQ03	1~7				8~9					9~12	107
SQ04	1~7		9~12								25
SQ05	1~7				5~12						45
SQ06	1~7		9~12	1	2~9					9~12	96
SQ07	1~7			9~12	1~8		7~8	7~8		9~12	93
SQ08	1~7	8~12		1~8	8~9					9~12	82
SQ09	1~7		9~12	1~8	9~12						37
SQ10		1~8			7~12	1~9	7~12	1~8		9~12	67
SQ11	1~7			9~12					1~8	9~12	49
SQ12	1~7		9~12								25
SQ13	1~7	8~12									12
SQ14	1~7				6 8~9					9~12	106
SQ16	1~7	7~8			3~8	9~12					53
SQ17							1~8			9~12	36
SQ18							1~8	1	9~12		23
SQ19							1~8			9~12	36
SQ20							1~8			9~12	36
SQ21							1~8			9~12	36
						Ali network					
Ail	1~7		9~12	1~8				1~8	8~12		40
Ali01	1~7	8~12	1~8		8				8~12		82

https://doi.org/10.5194/essd-2020-209
Preprint. Discussion started: 16 October 2020

Ali02	**1~7 11~12**	**1~8**			**8**				**8~12**		**85**
Ali03	**1~7**			**3~12**	**1~8**				**8~12**		**78**

Table 5. Same as the Table 3 but for the Naqu network.

	2010	**2011**	**2012**	**2013**	**2014**	**2015**	**2016**	**2017**	**2018**	**2019**	**Data length (months)**
Naqu	**1~7**			**8~9**	**6~8**	**6~9**		**9~12**	**1~8**	**9~12**	**88**
East		**1~8**		**9~12**							**24**
West	**1~7**	**1~8**		**1~9**	**7~12**	**1~7**	**8~12**				**42**
North		**1~8 11~12**	**1~3 9**	**9~12**			**1~8**	**9~12**	**1~8**	**9~12**	**42**
South		**1~8**	**9~12**								**12**
Kema				**1~9**	**3~9**		**8~12**				**26**
MS	**1~7**		**10~12**	**1~9**	**8~9 11~12**	**1~5**		**9~12**	**1~8**	**9~12**	**76**
NQ01									**1~8**	**9~12**	**12**
NQ02									**1~8**	**9~12**	**12**
NQ03							**1~8**	**9~12**	**1~8**	**9~12**	**24**
NQ04									**1~8**	**9~12**	**12**

Table 6. Evaluated metrics computed for the upscaled SM produced by the four upscaling methods with input of the maximum available monitoring sites.

Methods	Maqu			Shiquanhe		
	MRD	σ(RD)	CEC	MRD	σ(RD)	CEC
AA-max	0.009	0.054	**0.055**	0.012	0.046	**0.047**
TS-max	0.022	0.089	0.092	0.011	0.114	0.114
VD-max	-0.026	0.064	0.069	-0.042	0.033	0.053
ATI-max	-0.005	0.145	0.145	0.016	0.068	0.070

Table 7. Error statistics computed between the SM obtained by the four upscaling methods with input of minimum available sites and the SM_{truth} produced by the AA-max for the Maqu and Shiquanhe networks.

	Bias ($m^3 m^{-3}$)	RMSE($m^3 m^{-3}$)	ubRMSE($m^3 m^{-3}$)	NSE
		Maqu		
AA-min	0.005	0.022	0.021	0.954
TS-min	0.025	0.050	0.044	0.747
VD-min	-0.007	0.022	0.020	0.954
ATI-min	-0.052	0.099	0.084	0.030
		Shiquanhe		
AA-min	0.010	0.011	0.005	0.816

https://doi.org/10.5194/essd-2020-209
Preprint. Discussion started: 16 October 2020

TS-min	-0.001	0.013	0.013	0.768
VD-min	0.019	0.020	0.006	0.400
ATI-min	-0.001	0.021	0.021	0.393

Table 8. Error statistics computed between the $SM_{AA\text{-}min}$ and the three model-based SM products for the Maqu and Shiquanhe networks.

	Bias ($m^3 m^{-3}$)	RMSE ($m^3 m^{-3}$)	Bias ($m^3 m^{-3}$)	RMSE ($m^3 m^{-3}$)
	Warm season		Cold season	
		Maqu		
ERA5-land	0.050	0.067	-	-
GLDAS Noah	-0.112	0.125	-0.049	0.088
MERRA2	-0.113	0.124	0.006	0.097
		Shiquanhe		
ERA5-land	0.002	0.079	-	-
GLDAS Noah	0.010	0.116	0.052	0.058
MERRA2	0.054	0.069	0.049	0.053

Table 9. Percentages of each combination's RMSE fall into different levels of defined RMSE standard.

RMSE	0.004	0.006	0.008	0.010	0.012	0.014	0.016	0.018	0.020
				Maqu network					
n=1 (%)									
n=2 (%)								0.74	3.68
n=3 (%)						0.44	1.32	3.97	7.79
n=4 (%)					0.21	1.05	3.74	9.16	16.93
n=5 (%)				0.03	0.58	3.10	9.31	18.23	28.18
n=6 (%)				0.09	1.87	8.27	19.18	31.22	42.36
n=7 (%)				0.69	6.21	18.11	31.91	43.98	54.32
n=8 (%)			0.08	3.29	14.97	30.32	43.97	55.36	64.79
n=9 (%)			0.84	9.58	26.27	42.42	55.47	65.94	74.16
n=10 (%)		0.01	3.91	19.74	38.94	54.41	66.13	75.21	82.23
n=11 (%)		0.53	11.10	32.92	51.7	65.66	75.9	83.32	88.87
n=12 (%)		3.52	23.95	47.3	64.03	75.87	84.45	90.14	94.30
n=13 (%)	0.29	13.82	39.87	61.81	75.67	85.38	91.55	95.38	97.77
n=14 (%)	3.68	32.35	57.79	74.85	86.47	92.79	96.91	98.82	99.41
n=15 (%)	21.32	56.62	75.00	88.97	95.59	98.53	99.26	100.00	100.00
n=16 (%)	52.94	82.35	94.12	94.12	100.00	100.00	100.00	100.00	100.00
				Shiquanhe network					
n=1 (%)							8.33	16.67	25.00
n=2 (%)		1.52	1.52	4.55	13.64	30.30	37.88	42.42	48.48
n=3 (%)		6.82	21.36	25.45	33.18	42.73	53.18	59.55	65.00

https://doi.org/10.5194/essd-2020-209
Preprint. Discussion started: 16 October 2020

n=4 (%)	1.62	11.31	29.7	41.41	51.11	57.37	63.23	70.51	77.58
n=5 (%)	3.66	23.11	36.87	49.12	60.23	68.18	76.14	82.32	88.26
n=6 (%)	11.36	30.95	44.37	59.85	70.24	79.11	85.28	90.15	93.29
n=7 (%)	20.20	39.77	56.06	68.31	77.90	86.87	93.43	96.84	98.48
n=8 (%)	29.29	50.51	62.63	77.58	89.09	96.57	97.98	98.99	99.60
n=9 (%)	33.64	59.55	82.73	91.36	96.36	98.18	99.55	99.55	100.00
n=10 (%)	48.48	78.79	92.42	96.97	96.97	100.00	100.00	100.00	100.00
n=11 (%)	83.33	91.67	100.00	100.00	100.00	100.00	100.00	100.00	100.00

Table 10. The combinations of sites ranked by RMSE values of SM at the Maqu network.

Rank	Site1	Site2	Site3	Site4	Site5	Site6	Site7	Site8	Site9	Site10	Site11	Site12	**RMSE**
1	CST01	CST02	NST02	NST03	NST04	NST05	NST06	NST07	NST10	NST13	NST14	NST15	0.00402
2	CST01	CST02	CST04	NST01	NST02	NST03	NST04	NST05	NST06	NST07	NST13	NST15	0.00417
3	CST02	NST01	NST02	NST03	NST04	NST05	NST06	NST07	NST10	NST13	NST14	NST15	0.00450
4	CST01	CST02	NST01	NST02	NST03	NST04	NST05	NST06	NST07	NST13	NST14	NST15	0.00450
5	CST01	CST02	CST03	NST02	NST03	NST04	NST05	NST06	NST07	NST10	NST14	NST15	0.00451
96	CST01	CST02	CST03	CST04	CST05	NST03	NST06	NST10	NST11	NST13	NST14	NST15	0.00555
97	CST01	CST02	CST03	NST01	NST02	NST04	NST05	NST06	NST11	NST13	NST14	NST15	0.00555
98	CST01	CST02	CST03	CST04	CST05	NST01	NST02	NST05	NST06	NST10	NST11	NST15	0.00556
99	CST03	NST02	NST03	NST04	NST05	NST06	NST07	NST10	NST11	NST13	NST14	NST15	0.00557
100	**CST02**	**CST03**	**CST05**	**NST01**	**NST03**	**NST05**	**NST06**	**NST10**	**NST11**	**NST13**	**NST14**	**NST15**	**0.00557**

Appendix A

A.1 Arithmetic averaging

The arithmetic averaging method assigns an equal weight coefficient to each SM monitoring site of the network, which can be formulated as:

$$\boldsymbol{\overline{\theta}_t^{ups}} = \frac{\mathbf{1}}{\boldsymbol{N}}\sum_{\boldsymbol{i=1}}^{\boldsymbol{N}} \boldsymbol{\theta_{t,i}^{obs}} \tag{A1}$$

where i represents the i^{th} SM monitoring site.

A.2 Voronoi diagram

The Voronoi diagram method divides the network area into several parts according to the distances between each SM monitoring site. This approach determines the weight of each site (w_i [-]) based on the geographic distribution of all the SM monitoring sites within the network area, which can be formulated as:

$$\boldsymbol{\overline{\theta}_t^{ups}} = \frac{\sum_{i=1}^{N} w_i \theta_{t,i}^{obs}}{\sum_{i=1}^{N} w_i} \tag{A2}$$

https://doi.org/10.5194/essd-2020-209
Preprint. Discussion started: 16 October 2020

A.3 Time stability

The time stability method is based on the assumption that the spatial SM pattern over time tends to be consistent (Vachaud et al., 1985), and the most stable site can be regarded as the representative site of the network. For each SM monitoring site i within the time window (M days in total), the mean relative difference MRD_i [-] and standard deviation of the relative difference $\sigma(RD_i)$ [-] are estimated as:

$$\sigma(RD_i) = \sqrt{\frac{1}{M-1}\sum_{t=1}^{M}(RD_{t,i} - MRD_i)^2} \tag{A3}$$

$$MRD_i = \frac{1}{M}\sum_{t=1}^{M}\frac{\theta_{t,i}^{obs} - \overline{\theta_t^{obs}}}{\overline{\theta_t^{obs}}} \tag{A4}$$

$$RD_{t,i} = \frac{\theta_{t,i}^{obs} - \overline{\theta_t^{obs}}}{\overline{\theta_t^{obs}}} \tag{A5}$$

where $\theta_{t,i}^{obs}$ [m^3 m^{-3}] represents the SM measured on the t^{th} day at the i^{th} monitoring site, $\overline{\theta_t^{obs}}$ [m^3 m^{-3}] represents the mean SM measured at all available monitoring sites on the t^{th} day. MRD_i quantifies the bias of each SM monitoring site to identify a particular location is wetter or drier than regional mean, and $\sigma(RD_i)$ characterizes the precision of the SM measurement. Jacobs et al., (2004) combined above two statistical metrics as a comprehensive evaluation criterion (CEC_i [-]):

$$CEC_i = \sqrt{(MRD_i)^2 + \sigma(RD_i)^2} \tag{A6}$$

On the basis of the rank - ordered CEC_i of all monitoring sites, the most stable site is identified by the lowest CEC_i value.

A.4 Apparent thermal inertia

The apparent thermal inertia method is based on the close relationship between apparent thermal inertia (τ [K^{-1}]) and SM(θ [m^3 m^{-3}]) (Van doninck et al., 2011; Veroustraete et al., 2012). If the true areal SM ($\bar{\theta}_t^{tru}$ (m^3 m^{-3})) is available, then the weight vector β can be derived by the ordinary least-squares (OLS) method that minimizes the cost function J as:

$$J = \sum_{t=1}^{M}(\theta_t^{tru} - \beta^T\theta_t^{obs})^2 \tag{A7}$$

However, the θ_t^{tru} [m^3 m^{-3}] is usually not available in practice, and the representative SM ($\bar{\theta}_t^{rep}$ [m^3 m^{-3}]) is thus introduced that contains random noise but with no bias. Since the OLS method may results in overfitting with usage of the $\bar{\theta}_t^{rep}$, a regularization term is introduced and Eq. (A7) can be re-formulated as (Tarantola, 2005):

$$J = \sum_{t=1}^{M}(\bar{\theta}_t^{rep} - \beta^T\theta_t^{obs})\sigma^{-2}(\bar{\theta}_t^{rep} - \beta^T\theta_t^{obs}) + \alpha\beta^T\beta \tag{A8}$$

where σ [m^3 m^{-3}] represents the standard deviation of $\bar{\theta}_t^{rep}$, α [-] is the regularization parameter.

The core issue of the ATI approach is to obtain the $\bar{\theta}_t^{rep}$ and minimize the cost function of Eq. (A8). The $\bar{\theta}_t^{rep}$ can be retrieved from the apparent thermal inertia τ by the empirical regression, and τ has strong connection with the surface status, e.g. land surface temperature and albedo, which is defined as:

$$\tau = C\frac{1-a}{A} \tag{A9}$$

https://doi.org/10.5194/essd-2020-209
Preprint. Discussion started: 16 October 2020

where C [-] represents the solar correction factor, a [-] represents the surface albedo, and A [K] represents the amplitude of the diurnal temperature cycle. The detailed description of the ATI approach is referred to Qin et al. (2013).

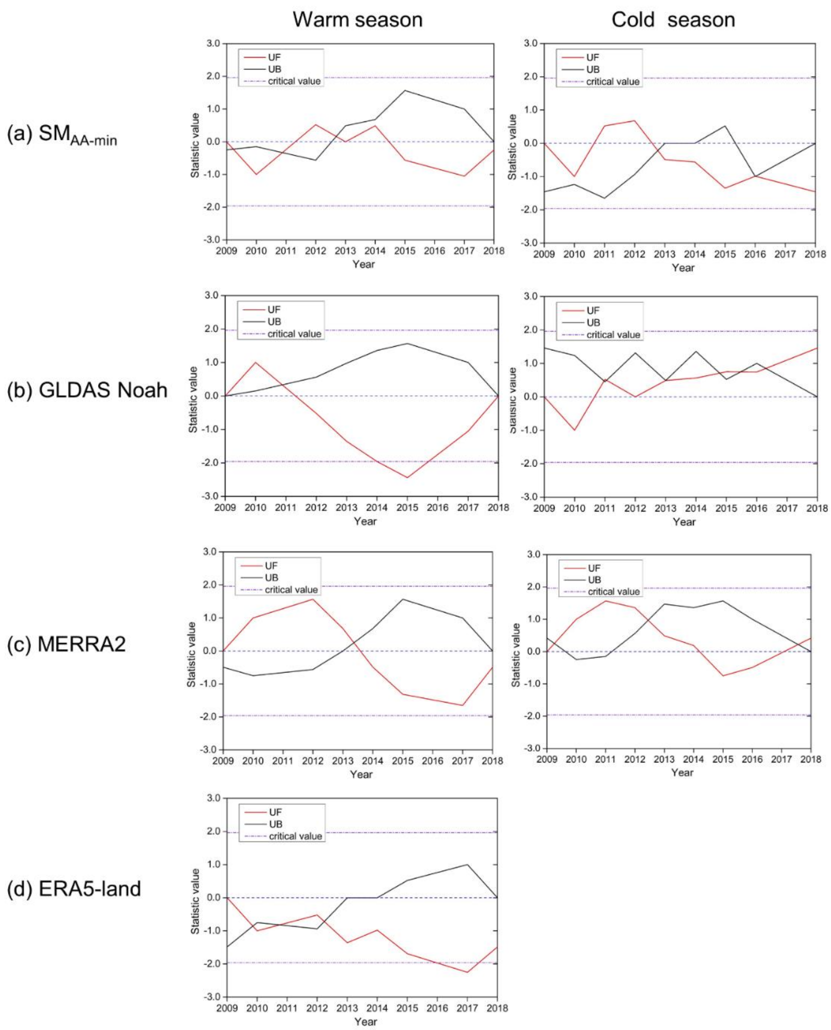

715

Fig. A1. M-K trend analysis of the (a) upscaled SM (SM_{AA-min}), and model-based SM derived from (b) GLDAS Noah (c) MERRA2, and (d) ERA5-land products for both warm and cold seasons at the Maqu network in a 10-year period.

https://doi.org/10.5194/essd-2020-209
Preprint. Discussion started: 16 October 2020

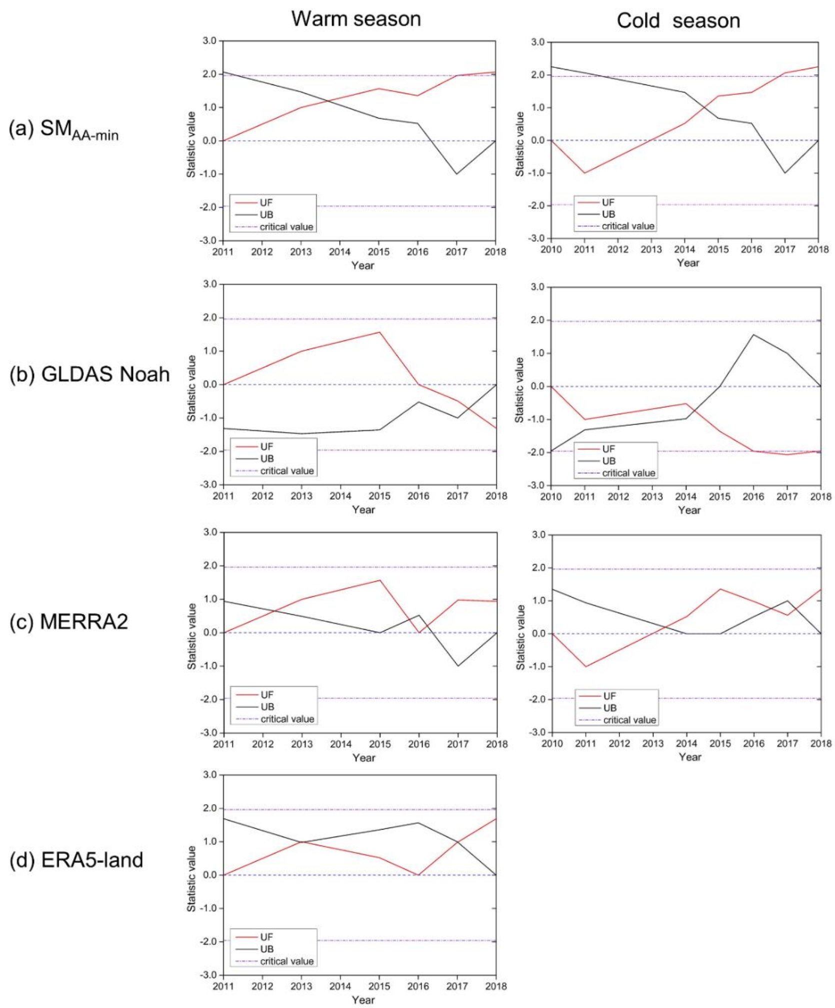

Fig. A2. Same as Fig. A1 but for the Shiquanhe network

Table A1. Soil moisture with temporal persistence for the Maqu network. Green shaded cells represent that there is not data missing, yellow shaded cells represent there is data missing with little influence.

Time	2009.11~ 2010.11	2010.11.~ 2011.11	2011.11~ 2012.11	2012.11~ 2013.11	2013.11~ 2014.11	2014.11~ 2015.11	2015.11~ 2016.11	2016.11~ 2017.11	2017.11~ 2018.11
CST05									
NST01									
NST03									
NST06									
NST07									
NST13									

https://doi.org/10.5194/essd-2020-209
Preprint. Discussion started: 16 October 2020

Open Access Earth System Science Data Discussions

NST01									
NST14									
CST03									
NST05									
CST01									
CST04									
NST02									
NST04									
CST02									
NST10									
NST15									
Valid stations	**17**	**14**	**10**	**8**	**6**	**6**	**4**	**3**	**3**

Table A2. Same as Table A1 but for the Shiquanhe network.

Time	**2010.8~ 2011.8**	**2011.8~ 2012.8**	**2012.8~ 2013.8**	**2013.8~ 2014.8**	**2014.8~ 2015.8**	**2015.8~ 2016.8**	**2016.8~ 2017.8**	**2017.8~ 2018.8**	**2018.8~ 2019.8**
SQ02									
SQ03									
SQ06									
SQ14									
SQ08									
SQ07									
SQ17									
SQ19									
SQ20									
SQ21									
SQ10									
SQ11									
Valid stations	**4**	**4**	**4**	**5**	**6**	**6**	**10**	**11**	**12**